On Effective Secrecy Throughput of Underlay Spectrum Sharing $\alpha - \mu$/ Málaga Hybrid Model Under Interference-and-Transmit Power Constraints

Md. Ibrahim, A. S. M. Badrudduza, *Graduate Student Member, IEEE*, Md. Shakhawat Hossen, M. K. Kundu, *Graduate Student Member, IEEE*, Imran Shafique Ansari, *Senior Member, IEEE*, and Imtiaz Ahmed, *Member, IEEE*

***Abstract*—The underlay cognitive radio-based hybrid radio frequency/free-space optical (RF/FSO) systems have emerged as a promising technology due to their ability to eliminate spectrum scarcity and spectrum under-utilization problems. The physical layer security of such a network with a primary user, a secondary source, a secondary receiver, and an eavesdropper is therefore examined in this work. In this network, secret communication occurs between two reliable secondary peers over the RF and FSO links simultaneously, and the eavesdropper can only overhear the RF link. In particular, the maximum transmits power limitation at the secondary user as well as the permissible interference power restriction at the primary user are also taken into consideration. All the RF and FSO links are modeled with α-μ fading and Málaga turbulence with link blockage and pointing error impairments. At the receiver, the selection combining diversity technique is utilized to select the signal with the best electrical signal-to-ratio (SNR). Furthermore, to examine the secrecy performance taking into account the effects of each system parameter, closed-form expressions for the secrecy outage probability and effective secrecy throughput are derived. The resultant expressions are finally verified by Monte-Carlo simulations.**

***Index Terms*—Cognitive underlay network, effective secrecy throughput, hybrid RF/FSO system, Málaga turbulence, pointing error, secure outage probability.**

I. Introduction

A. Background and Related Works

With the rapid increase in wireless devices, the shortage of spectrum owing to the data traffic reflects a significant threat in contemporary technology [1], [2]. In order to meet the requirements, several optimistic technologies have been developed recently. Among these, both cognitive radio network (CRN) and free-space optical (FSO) systems have received considerable attention from the research communities [3], [4]. Although FSO communication appears with specific merits, such as high bandwidth, inherent security, and cost-effective operation, several issues like atmospheric turbulence and pointing error can affect the secure transmission greatly [5]. Furthermore, the probability of transmission blockage due to extreme line-of-site (LOS) necessity in FSO link leads to the system failure [6]. Hence, utilizing radio frequency (RF) technology as an alternative option along with the FSO system assures successful transmission since the FSO link delivers high data speed while the RF link is independent of the atmospheric turbulence and weather conditions [7].

Due to the increased demand for faster data rates in wireless communication, hybrid networks, which consist of RF and FSO systems, are deployed utilizing a variety of techniques. An adaptive coding method in order to enhance the system performance of RF/FSO hybrid network was considered in [8], [9]. Nonetheless, the performance of these systems is highly dependent on the existence of feedback information at the receiver [9]. Another attractive feature is the switching mechanism that uses RF link when FSO link is down [10]. Since one link is underutilized at a time, there is a significant amount of bandwidth wasted [11]. To extend the communication range, several existing works like [12], [13], [14], [15] utilize relaying protocols in mixed RF-FSO models. However, weather conditions (i.e. fog) can influence the performance of dual-hop networks badly. Unlike [10], [11], the considered hybrid RF/FSO model dispatches identical information via two separate links simultaneously and combines the received signal using the diversity combining method. Again, the mixed RF-FSO system differs completely from the hybrid RF/FSO model in terms of system configuration. Recently, a comprehensive analysis on hybrid RF/FSO model was performed in [16], [17] where the hybrid system exhibits better link availability compared to the individual links.

In CRN, an unlicensed user gets the permission of accessing the same spectrum of the licensed user through different spectrum sharing methods [18]. More particularly, in the underlay approach, the secondary user (SU) makes use of the

Manuscript received 25 October 2022; revised 13 February 2023; accepted 27 February 2023. Date of publication 6 March 2023; date of current version 22 March 2023. This work was supported by the Start-Up Research Grant of the Department of Electrical Engineering and Computer Science at Howard University, Washington, DC, USA. *(Corresponding author: Md. Ibrahim.)*

Md. Ibrahim is with the Institute of ICT, Rajshahi University of Engineering & Technology (RUET), Kazla, Rajshahi 6204, Bangladesh (e-mail: ibrahim-ruet.007@gmail.com).

A. S. M. Badrudduza and Md. Shakhawat Hossen are with the Department of ETE, RUET, Kazla, Rajshahi District 6204, Bangladesh (e-mail: asmb.kanon@gmail.com; shakhawat.czs@gmail.com).

M. K. Kundu is with the Department of ECE, RUET, Kazla, Rajshahi District 6204, Bangladesh (e-mail: mkkeee002@gmail.com).

Imran Shafique Ansari is with the James Watt School of Engineering, University of Glasgow, Glasgow G12 8QQ, U.K. (e-mail: ansarimrans@gmail.com).

Imtiaz Ahmed is with the Department of Electrical Engineering and Computer Science, Howard University, Washington, DC 20059 USA (e-mail: imtiaz.ahmed@howard.edu).

Digital Object Identifier 10.1109/JPHOT.2023.3253020

primary user's (PU) shared spectrum as long as the interference occurring at SU is less than the permitted threshold value [4]. Considering CR technology in the RF links, the system performance of mixed RF-FSO systems are investigated in [4], [18], [19], [20], [21], [22]. In [20], the performance analysis was accomplished by developing analytical expressions of outage probability (OP) where RF-FSO links were subjected to Nakagami-m fading and double generalized Gamma (DGG) turbulence, respectively. However, this model was extended in [18], [21] where the impact of antenna diversity in RF links was observed. In [22], the OP analysis was performed for amplify-and-forward (AF) relaying-based dual-hop network while multi-users and multi-destination were taken into consideration. The error probability (EP) expression was derived in [4] where the influence of RF and FSO parameters on the system performance was inspected.

Security has become a widespread concern in next-generation wireless communications (5G and beyond) due to its high risk of information leakage [23], [24], [25]. In this domain, physical layer security (PLS) has been recognized as a complementary choice to the traditional cryptography strategy [26], [27]. According to the comprehensive literature analysis, current PLS research has mainly been limited to hybrid RF/FSO models [26], [28], [29] and mixed RF-FSO networks [30], [31], [32]. In [26], the PLS of a hybrid FSO/RF network was examined and it was found that secrecy performance is highly dependent on air turbulence, pointing error, and RF fading parameters. In [28], authors obtained the secrecy diversity gain for the RF backhaul system along with parallel FSO link whereas the impact of power allocation on secrecy performance was investigated in [29] for the parallel mmWave and FSO links. Including link blockage (LB) probability in the FSO link due to the sudden presence of moving objects (e.g. clouds, birds, insects, etc.), [33] introduced the strategy of enhancing secrecy behavior for CR-based hybrid RF/FSO system.

B. Motivation and Contributions

While a CR-based hybrid RF/FSO system configuration is more robust and practical than a single RF or FSO link [28], there have been only a few studies focused on its secrecy analysis. The authors of [26], [28], [34], [35] evaluated the security of hybrid RF-FSO models but did not take into account CR technology with power constraints. As a result, the investigation of PLS in a CR-based hybrid model remains an open concept. To the best of our knowledge, there are no studies that have looked into the secrecy analysis of a hybrid CR RF/FSO system while considering both the transmit power constraints at the SU and the maximum allowable interference power at the PU. To address this research gap, we investigate the security performance of an underlay CR-based hybrid RF/FSO fading channel in the presence of an eavesdropper. We consider the generalized α-μ fading channel for RF links and the Málaga ($\mathcal{M}$) distribution for the FSO link. Special consideration was made while choosing these channel models. In a hybrid RF/FSO system, small-scale fading can have a significant impact on communication performance and the alpha-mu fading channel is a generalized model that can describe small-scale fading perfectly [36]. On the other hand, pointing error and atmospheric turbulence are two very important parameters in the FSO channel and these two parameters can be perfectly represented by $\mathcal{M}$ distribution [37]. Both these channel links are flexible, as they can describe a variety of fading scenarios by adjusting their parameters. Our study also includes both the single power constraint and the double power constraint. The contributions of this work are highlighted as follows:

1) Firstly, the expressions of cumulative density function (CDF) for selection combining (SC) based hybrid cognitive spectrum-sharing RF/FSO network assuming two different scenarios (e.g. single and double power constraints) are derived in closed form. It is noteworthy that most of the works in the literature explored the secrecy behavior of the CR RF/FSO schemes considering maximum interference power constraint at PU only. However, this research takes into account the power limits at both SU and PU, which distinguishes this model from those previously investigated models and makes it more reliable. From this perspective, a hybrid model of this kind is undoubtedly new and more useful. Moreover, this expression of CDF also incorporates some other existing works [16], [17], [26], [28], [33] as special cases.
2) Secondly, the secrecy characteristics are derived for the proposed system model utilizing the underlay approach over the RF links and developing the analytical expressions for secrecy outage probability (SOP), probability of strictly positive secrecy capacity (SPSC), and effective secrecy throughout (EST) for the two scenarios. Since the considered $\alpha-\mu$ and Málaga models are generalized, and combination of the two in such type of hybrid model has been considered for the first time in the literature, according to the authors' knowledge, the derived expressions are also novel and generalized.
3) The derived expressions are further utilized to realize some numerical outcomes with some specific figures demonstrating the impacts of each system parameter i.e. fading, primary-secondary interference, LB probability, pointing error, detection techniques, and various atmospheric turbulence conditions, etc. It is also notable that both detection techniques, i.e. heterodyne detection (HD) and intensity modulation/direct detection (IM/DD) techniques, have not been considered yet in such type of hybrid system model except in this work. It should be highlighted that as atmospheric turbulence, pointing error, and link blockage probability rise, the security of the systems is compromised. By adopting the HD approach over IM/DD and carefully adjusting the system's fading parameters, this issue can be mitigated. Finally, the accuracy of the deduced analytical expressions is corroborated via Monte-Carlo (MC) simulations.

C. Organization

The outline of this paper is arranged as follows: In Sections-II, III, and IV, the proposed framework along with the channel models is described. The novel analytical expressions of the performance metrics (i.e. SOP, probability of SPSC, and EST analysis for the two scenarios) are demonstrated in Section-V.

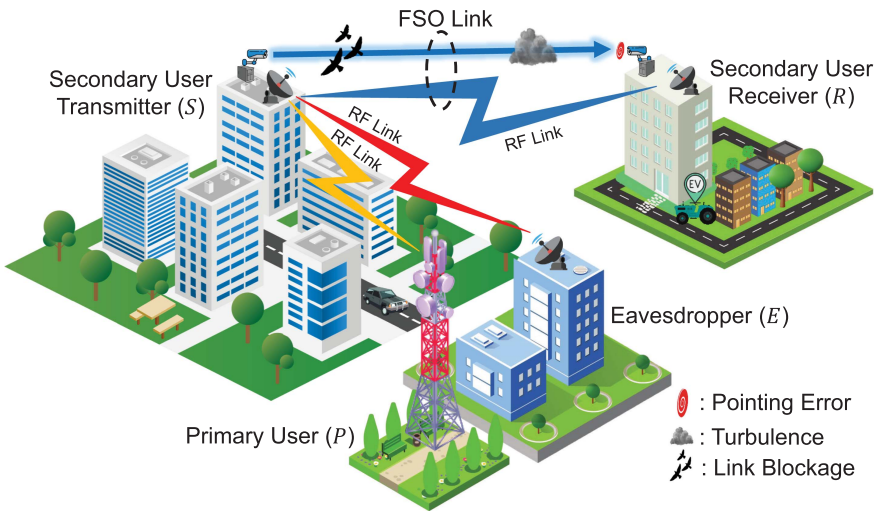

Fig. 1. Proposed system model for hybrid RF/FSO based cognitive underlay network.

Section-VI incorporates some exclusive numerical results followed by insightful discussions. Finally, the concluding remarks of this work are presented in Section-VII.

II. System Model

A hybrid cognitive underlay network (CUN) is illustrated in Fig. 1, which incorporates two parallel links: cognitive RF and FSO sub-systems, respectively in order to transmit confidential information from a secondary user transmitter S to a receiver R in the presence of an eavesdropper E. It is essential to mention that FSO communication allows the benefits of using a license-free spectrum with high data rates and low latency [12]. The FSO subsystem, however, experiences substantial interruptions in signal transmission due to atmospheric turbulence, aiming inaccuracies, and obstructions along the link, making the communication system dependent on weather conditions. Hence, the RF sub-system is utilized to transmit the same information concurrently with the FSO sub-system ensuring a constant flow of data. To prevent any data loss, R exploits selection combining diversity and always picks the best signal, i.e. the signal with the highest (signal-to-noise ratio) SNR, among the two sub-links. The proposed underlay technique involves the use of the licensed spectrum of the primary user (P) by S, and therefore, the system mandates that there must not be any harmful interference to P.

1) Cognitive RF Sub-Link: Based on the underlay approach, S transmits its concealed information to R under the following constraints:

- The peak tolerable interference power impinged by S on P cannot exceed a predefined value P_Q. In such a case, S is not considered as a power limited terminal and it has the full freedom to utilize its power depending on a single power constraint, i.e. interference severity at P. This particular case is denoted as *Scenario-I* in the rest of this work.
- The CUN in *Scenario-I* sometimes may not be practical, specifically when the channel coefficient of $S-P$ link rapidly fluctuates. This may lead to a feedback burden since the instantaneous feedback gain is difficult to track. To mitigate these types of feedback burden and feedback errors, mean value power allocation strategy can be adopted [38]. Hence, besides only interference/single power constraint case, in the double power constraint case, S is assumed to be a power-limited terminal and allowed to exploit maximum transmit power P_T. This particular case is denoted as *Scenario-II* in the remaining manuscript.

For *Scenario-II*, utilizing mean value power allocation, the transmit power of S is denoted as

$$P_{T,II} = \min\left(\frac{P_Q}{|g_p|^2}, P_T\right), \tag{1}$$

where g_p denotes the channel gain of $S-P$ interference link. Therefore, the SNR at R is expressed as

$$\gamma_{r,II} = \min\left(\frac{\Psi_Q}{|g_p|^2}, \Psi_T\right)|g_r|^2, \tag{2}$$

where $\Psi_Q = \frac{P_Q}{N_r}$, $\Psi_T = \frac{P_T}{N_r}$, N_r represents the noise power imposed on R, and g_r is the channel gain of $S-R$ RF sub-link. However, when S is not a power-limited terminal (*Scenario-I*), the transmit power at S is represented as

$$P_{t,I} = \frac{P_Q}{|g_p|^2}. \tag{3}$$

In this case, the SNR of $S-R$ RF sub-link is expressed as

$$\gamma_{r,I} = \frac{\Psi_Q|g_r|^2}{|g_p|^2}. \tag{4}$$

2) FSO Sub-Link: The FSO sub-system comprises of S with a transmit aperture, FSO sub-link, and R with a receive photo-detector. The transmitter dispatches information in optical form that is further converted into electrical one utilizing the photo-detector at R. Thereby, instantaneous SNR for $S-R$ FSO sub-link is written as

$$\gamma_o = \frac{P_f}{N_o}\|g_o\|^2, \tag{5}$$

where g_o signifies the channel gain of $S-R$ FSO sub-link, N_o denotes the optical noise power at R, and P_f is the transmit optical power at S.

Finally, after selection combining at R, the received SNR is written as [26, Eq. (11)]

$$\gamma_{f,j} = \max(\gamma_{r,j}, \gamma_o), \tag{6}$$

where $j \in \{I, II\}$.

3) Eavesdropper Link: In the proposed system, an eavesdropper (E) targets the RF sub-link to intercept the confidential data stream. The instantaneous SNR at E is expressed as

$$\gamma_{e,j} = \frac{P_{t,j}}{N_e}\|g_e\|^2, \tag{7}$$

where g_e denotes the channel gain of $S-E$ link and N_e is the noise power at E.

III. Channels Realization

In this section, the channel models of the $S-R$ (RF and FSO sub-links), $S-E$, and $S-P$ links are realized individually for further utilization in the mathematical modeling of the proposed CUN system.

A. PDF and CDF of SNRs for the RF Links

The $S-R$ RF sub-link, $S-P$, and $S-E$ links are assumed to follow $\alpha-\mu$ distribution, where α denotes the non-linearity parameter of propagation environment ($\alpha > 0$) and μ represents the number of multi-path clusters ($\mu > 0$). Since $\alpha-\mu$ model exhibits generalized characteristics [39], several multi-path models [40], e.g. exponential, Rayleigh, Weibull, Gaussian, Gamma, and Nakagami-m, etc., can be obtained by setting different values of α and μ. The PDF of γ_i, $i \in \{r, p, e\}$, where r, p, and e correspond to the $S-R$ (RF), $S-P$, and $S-E$ links, respectively, is given as [41, Eq. (2)]

$$f_{\gamma_i}(\gamma) = \frac{\alpha_i \delta_i^{\mu_i}}{2\Gamma(\mu_i)} e^{-\delta_i \gamma^{\tilde{\alpha_i}}} \gamma^{\Theta_i}. \tag{8}$$

Here $\delta_i = \Phi_i^{-\tilde{\alpha_i}}$, $\Theta_i = \tilde{\alpha_i}\mu_i - 1$, $\tilde{\alpha_i} = \frac{\alpha_i}{2}$, Φ_i is the average SNR of the RF links, and $\Gamma(\cdot)$ denotes the Gamma operator. The CDF of γ_i is defined as

$$F_{\gamma_i}(\gamma) = \int_0^{\gamma} f_{\gamma_i}(\gamma) d\gamma. \tag{9}$$

Plugging (8) into (9), and after performing integration upon utilizing [42, Eq. (3.381.8)], the CDF leads to

$$F_{\gamma_i}(\gamma) = \frac{\gamma(\mu_i, \delta_i \gamma^{\tilde{\alpha_i}})}{\Gamma(\mu_i)}, \tag{10}$$

where $\gamma(.,.)$ denotes the lower incomplete Gamma function. Finally, with the help of [42, Eq. (8.352.6)], the CDF of γ_i can be expressed in an alternative form as

$$F_{\gamma_i}(\gamma) = 1 - e^{-\delta_i \gamma^{\tilde{\alpha_i}}} \sum_{m_i=0}^{\mu_i - 1} \frac{(\delta_i \gamma^{\tilde{\alpha_i}})^{m_i}}{m_i!}. \tag{11}$$

B. PDF and CDF of SNR for FSO SUB-Link

The $S-R$ FSO sub-link is considered to follow Málaga ($\mathcal{M}$) turbulence. Since Málaga turbulence is a generalized FSO model, it incorporates some other popular models, such as Gamma-Gamma, lognormal, Rice-Nakagami, K distribution and Gamma as special cases [43], [44]. Hence, the PDF of γ_o is expressed as [45, Eq. (9)]

$$f_{\gamma_o}(\gamma) = \frac{\epsilon^2 \chi_o}{2^s \gamma} \sum_{m_o=0}^{\beta_o} \vartheta_n G_{1,3}^{3,0}\left[\varpi\left(\frac{\gamma}{\mu_s}\right)^{\frac{1}{s}} \middle| \begin{matrix} \epsilon^2+1 \\ \epsilon^2, \alpha_o, m_o \end{matrix}\right], \tag{12}$$

where

$$\chi_o = \frac{2\alpha_o^{\frac{\alpha_o}{2}}}{g^{1+\frac{\alpha_o}{2}}\Gamma(\alpha_o)}\left(\frac{g\beta_o}{g\beta_o + \Omega_o}\right)^{\beta_o + \frac{\alpha_o}{2}},$$

$$\varpi = \frac{\epsilon^2 \alpha_o \beta_o (g + \Omega_o)}{(\epsilon^2+1)(g\beta_o + \Omega_o)},$$

$$\vartheta_n = \upsilon_n \left(\frac{\alpha_o \beta_o}{g\beta_o + \Omega_o}\right)^{-\frac{\alpha_o + m_o}{2}},$$

$$\upsilon_n = \binom{\beta_o - 1}{m_o - 1} \frac{(g\beta_o + \Omega_o)^{1-\frac{m_o}{2}}}{(m_o - 1)!}\left(\frac{\Omega_o}{g}\right)^{m_o - 1}\left(\frac{\alpha_o}{\beta_o}\right)^{\frac{m_o}{2}},$$

α_o and β_o denote the fading parameters, $g = 2b_o(1-\rho)$ represents the average power of scattering components received through off-axis eddies, $2b_o$ denotes the total average power of scattering components, ϵ ($0 \le \rho \le 1$) signifies the amount of scattering power coupled to the LOS component, the average power realized from coherent contributions is symbolized by $\Omega_o = \acute{\Omega_o} + 2b_o\rho + 2\sqrt{2b_o\rho\acute{\Omega_o}}\cos(\phi_A - \phi_B)$, $\acute{\Omega_o}$ is termed as the average power of LOS components, ϕ_A and ϕ_B represent the deterministic phases of LOS, $\mu_1 = \Phi_o$, $\mu_2 = \frac{\alpha_o \epsilon^2 (\epsilon^2+1)^{-2}(\epsilon^2+2)(g+\Omega_o)\Phi_o}{(\alpha_o+1)[2g(g+2\Omega_o)+\Omega_o^2(1+1/\beta_o)]}$, s denotes the detection technique (i.e. $s=1$ refers to HD technique and $s=2$ refers to IM/DD technique), Φ_o denotes the average SNR of FSO sub-link that is related to electrical SNR μ_s, and G[·] represents the Meijer's G function [46]. Plugging (12) into (9), the CDF of γ_o is written as [45, Eq. 11]

$$F_{\gamma_o}(\gamma) = K \sum_{m_o=0}^{\beta_o} \varsigma_n G_{s+1,3\,s+1}^{3\,s,1}\left[\frac{V\gamma}{\mu_s} \middle| \begin{matrix} 1, q_1 \\ q_2, 0 \end{matrix}\right], \tag{13}$$

where $K = \frac{\epsilon^2 \chi_o}{2^s (2\pi)^{s-1}}$, $\varsigma_n = \vartheta_n s^{\alpha_o + m_o - 1}$, $V = \frac{\varpi^s}{s^{2s}}$, $q_1 = \{\frac{\epsilon^2+1}{s}, \ldots, \frac{\epsilon^2+s}{s}\}$ including s number of terms, and $q_2 = \{\frac{\epsilon^2}{s}, \ldots, \frac{\epsilon^2+s-1}{s}, \frac{\alpha_o}{s}, \ldots, \frac{\alpha_o+s-1}{s}, \frac{m_o}{s}, \ldots, \frac{m_o+s-1}{s}\}$ including $3\,s$ number of terms.

The FSO link can be temporarily blocked due to its extreme LOS requirements. Hence, including link blocking probability (P_o) in FSO and assuming SNR of the $S-R$ FSO sub-link as γ_{o^*}, the PDF of γ_{o^*} is expressed finally as [6, Eq. (10)]

$$f_{\gamma_{o^*}}(\gamma) = P_o \delta(\gamma) + (1 - P_o) f_{\gamma_o}(\gamma), \tag{14}$$

where $\delta(\cdot)$ denotes a Dirac delta function [47, Eq. (14.03.02.0001.01)]. Now, the CDF of γ_{o^*} is expressed as

$$F_{\gamma_{o^*}}(\gamma) = \int_0^{\gamma} f_{\gamma_{o^*}}(\gamma) d\gamma \cong P_o + (1 - P_o) F_{\gamma_o}(\gamma). \tag{15}$$

Substituting (13) into (15), we obtain

$$F_{\gamma_{o^*}}(\gamma)=P_o+(1-P_o)K\sum_{m_o=0}^{\beta_o}\varsigma_n\, G_{s+1,3\,s+1}^{3\,s,1}\left[\frac{V\gamma}{\mu_s}\middle|\begin{matrix}1,q_1\\ q_2,0\end{matrix}\right]. \tag{16}$$

IV. Cognitive Underlay Network

This section demonstrates the CDFs of SNRs for the hybrid RF/FSO CUN considering both scenarios (Scenarios- I & II).

A. Scenario I

Considering the interference of $S-P$ link and denoting SNR of the $S-R$ RF sub-link as $\gamma_{r,I}$, the CDF of $\gamma_{r,I}$ is written as [4, Eq. (4)]

$$F_{\gamma_{r,I}}(\gamma)=\int_0^{\infty}F_{\gamma_r}\left(\frac{\gamma}{\Psi_Q}x\right)f_{\gamma_p}(x)dx. \tag{17}$$

Now substituting (11) and (8) into (17), the CDF is expressed further as

$$F_{\gamma_{r,I}}(\gamma)=1-\sum_{m_r=0}^{\mu_r-1}\frac{\alpha_p\delta_r^{m_r}\delta_p^{\mu_p}}{2\Gamma(\mu_p)m_r!}\left(\frac{\gamma}{\Psi_Q}\right)^{\tilde{\alpha_r}m_r}\times\int_0^{\infty}e^{-(\delta_p x^{\tilde{\alpha_p}}+\Xi_1^I\gamma_r^{\tilde{\alpha_r}}x^{\tilde{\alpha_r}})}x^{\Theta_p+\tilde{\alpha_r}m_r}dx, \tag{18}$$

where $\Xi_1^I=\delta_r\Psi_Q^{-\tilde{\alpha_r}}$. Now, following some algebraic manipulations, assuming $\tilde{\alpha_p}=\tilde{\alpha_r}$, and performing integration utilizing [42, Eq. (3.326.2)], the CDF of $S-R$ RF sub-link is finally obtained as

$$F_{\gamma_{r,I}}(\gamma)=1-\sum_{m_r=0}^{\mu_r-1}\frac{\Gamma(\Xi_2^I)\alpha_p\delta_r^{m_r}\delta_p^{\mu_p}}{\tilde{\alpha_p}2\Gamma(\mu_p)m_r!}\left(\frac{\gamma}{\Psi_Q}\right)^{\tilde{\alpha_r}m_r}\times(\Xi_1^I\gamma^{\tilde{\alpha_r}}+\Phi_p^{-\tilde{\alpha_p}})^{-\Xi_2^I}, \tag{19}$$

where $\Xi_2^I=\frac{\tilde{\alpha_r}m_r+\mu_p\tilde{\alpha_p}}{\tilde{\alpha_p}}$. According to (6), the CDF of end-to-end SNR at R is written as

$$F_{\gamma_{f,I}}(\gamma)=F_{\gamma_{r,I}}(\gamma)\times F_{\gamma_{o^*}}(\gamma). \tag{20}$$

By replacing (19) and (16) into (20), the CDF of $\gamma_{f,I}$ is derived in (21) shown at the bottom of this page.

B. Scenario II

Assuming double power constraints in the RF sub-link, the CDF of $F_{\gamma_{r,II}}$ is written as

$$F_{\gamma_{r,II}}(\gamma_r)=\Pr\left\{\min\left(\frac{\Psi_Q}{|g_p|^2},\Psi_T\right)|g_r|^2\le\gamma_r\right\}$$
$$=\underbrace{\Pr\left\{|g_r|^2\le\frac{\gamma_r}{\Psi_T},\frac{\Psi_Q}{|g_p|^2}\ge\Psi_T\right\}}_{\Lambda_1}+\underbrace{\Pr\left\{\frac{|g_r|^2}{|g_p|^2}\le\frac{\gamma_r}{\Psi_Q},\frac{\Psi_Q}{|g_p|^2}\le\Psi_T\right\}}_{\Lambda_2}. \tag{22}$$

Since g_r and g_p are completely independent to one other, hence, Λ_1 is expressed in an alternative form as

$$\Lambda_1=\Pr\left\{|g_p|^2\le\frac{\Psi_Q}{\Psi_T}\right\}\Pr\left\{|g_r|^2\le\frac{\gamma_r}{\Psi_T}\right\}=F_{\gamma_p}\left(\frac{\Psi_Q}{\Psi_T}\right)F_{\gamma_r}\left(\frac{\gamma}{\Psi_T}\right). \tag{23}$$

Substituting (11) into (23), Λ_1 can be finally written as

$$\Lambda_1=1-\sum_{m_p=0}^{\mu_p-1}\Xi_1^{II}-\sum_{m_r=0}^{\mu_r-1}\Xi_2^{II}\gamma^{\tilde{\alpha_r}m_r}e^{-\delta_r\Psi_T^{-\tilde{\alpha_r}}\gamma^{\tilde{\alpha_r}}}+\sum_{m_p=0}^{\mu_p-1}\sum_{m_r=0}^{\mu_r-1}\Xi_3^{II}\gamma^{\tilde{\alpha_r}m_r}e^{-(\delta_p\Psi_Q^{\tilde{\alpha_p}}\Psi_T^{-\tilde{\alpha_p}}+\delta_r\Psi_T^{-\tilde{\alpha_r}}\gamma^{\tilde{\alpha_r}})}, \tag{24}$$

where $\Xi_1^{II}=\frac{\delta_p^{m_p}}{m_p!}\left(\frac{\Psi_Q}{\Psi_T}\right)^{\tilde{\alpha_p}m_p}e^{-\delta_p\Psi_Q^{\tilde{\alpha_p}}\Psi_T^{-\tilde{\alpha_p}}}$, $\Xi_2^{II}=\frac{\delta_r^{m_r}}{m_r!}\Psi_T^{-\tilde{\alpha_r}m_r}$, and $\Xi_3^{II}=\frac{\delta_p^{m_p}\delta_r^{m_r}}{m_r!m_p!}(\frac{\Psi_Q}{\Psi_T})^{\tilde{\alpha_p}m_p}\Psi_T^{-\tilde{\alpha_r}m_r}$. Now, according to the concept of probability theory [48], Λ_2 is written as

$$\Lambda_2=\int_{\frac{\Psi_Q}{\Psi_T}}^{\infty}f_{\gamma_p}(y)\int_0^{\frac{\gamma_r}{\Psi_Q}y}f_{\gamma_r}(x)dxdy=\int_{\frac{\Psi_Q}{\Psi_T}}^{\infty}f_{\gamma_p}(y)F_{\gamma_r}\left(\frac{\gamma y}{\Psi_Q}\right)dy. \tag{25}$$

Replacing (8) and (11) into (25), Λ_2 is obtained as

$$\Lambda_2=\Xi_5^{II}-\sum_{m_r=0}^{\mu_r-1}\sum_{m_3=0}^{\Omega-1}\sum_{m_4=0}^{m_3}\sum_{m_5=0}^{\infty}\binom{m_3}{m_4}\binom{\Omega+m_5-1}{m_5}\times\Xi_6^{II}\gamma^{\tilde{\alpha_r}(m_r+m_4+m_5)}e^{-(\delta_p\Psi_Q^{\tilde{\alpha_r}}\Psi_T^{-\tilde{\alpha_r}}+\delta_r\Psi_T^{-2\tilde{\alpha_r}}\Psi_Q^{-\tilde{\alpha_r}}\gamma^{\tilde{\alpha_r}})}, \tag{26}$$

where $\Xi_5^{II}=\frac{\alpha_p\delta_p^{\mu_p}}{2\Gamma(\mu_p)\tilde{\alpha_p}\delta_p^{\Xi_4^{II}}}\Gamma[\Xi_4^{II},\delta_p(\frac{\Psi_Q}{\Psi_T})^{\tilde{\alpha_p}}]$, $\Xi_4^{II}=\frac{\Theta_p+1}{\tilde{\alpha_p}}$, $\Omega=\frac{\Theta_p+\tilde{\alpha_r}m_r+1}{\tilde{\alpha_r}}$, and $\Xi_6^{II}=\frac{\alpha_p\delta_r^{m_r+m_4+m_5}(\Omega-1)!(-1)^{m_5}}{2\Gamma(\mu_p)m_r!\tilde{\alpha_r}m_3!}\delta_p^{-(\Omega+m_5-m_3+m_4-\mu_p)}\Psi_Q^{-\tilde{\alpha_r}(m_r-m_3+m_5)}(\Psi_T^{-\tilde{\alpha_r}})^{m_3+m_4}$. For proof, please see the Appendix. Finally, utilizing (24) and

$$F_{\gamma_{f,I}}(\gamma)=P_o+(1-P_o)\sum_{m_o=0}^{\beta_o}K\varsigma_nG_{s+1,3\,s+1}^{3\,s,1}\left[\frac{V\gamma}{\mu_s}\middle|\begin{matrix}1,q_1\\ q_2,0\end{matrix}\right]-P_o\sum_{m_r=0}^{\mu_r-1}\frac{\delta_r^{m_r}\alpha_p\delta_p^{\mu_p}\Gamma(\Xi_2^I)}{2\Gamma(\mu_p)\tilde{\alpha_p}m_r!}\left(\frac{\gamma}{\Psi_Q}\right)^{\tilde{\alpha_r}m_r}(\Xi_1^I\gamma^{\tilde{\alpha_p}}+\Phi_p^{-\tilde{\alpha_p}})^{-\Xi_2^I}$$
$$-(1-P_o)\sum_{m_r=0}^{\mu_r-1}\sum_{m_o=0}^{\beta_o}K\varsigma_n\frac{\Gamma(\Xi_2^I)\alpha_p\delta_p^{\mu_p}\delta_r^{m_r}}{\tilde{\alpha_p}2\Gamma(\mu_p)m_r!}\left(\frac{\gamma}{\Psi_Q}\right)^{\tilde{\alpha_r}m_r}(\Xi_1^I\gamma^{\tilde{\alpha_p}}+\Phi_p^{-\tilde{\alpha_p}})^{-\Xi_2^I}G_{s+1,3\,s+1}^{3\,s,1}\left[\frac{V\gamma}{\mu_s}\middle|\begin{matrix}1,q_1\\ q_2,0\end{matrix}\right]. \tag{21}$$

(26) into (22), and performing some simple mathematical operations, $F_{\gamma_{r,II}}(\gamma)$ is written as shown in (27) shown at the bottom of this page. Now, similar to (20), the CDF of $\gamma_{f,II}$ is expressed as

$$F_{\gamma_{f,II}}(\gamma) = F_{\gamma_{r,II}}(\gamma) \times F_{\gamma_{o^*}}(\gamma). \tag{28}$$

Now, substituting (27) and (16) into (28), the CDF of $\gamma_{f,II}$ is obtained as shown in (29) shown at the bottom of this page, where $\mathcal{X} = 1 + \Xi_5^{II} - \sum_{m_p=0}^{\mu_p-1} \Xi_1^{II}$.

V. Performance Analysis

In this section, we demonstrate the novel analytical expressions for SOP, probability of SPSC, and EST utilizing (8), (21), and (29).

A. Secure Outage Probability Analysis

In order to investigate the secrecy behavior of the proposed hybrid system, SOP is one of the fundamental performance metrics. SOP particularly depends on whether the target secrecy rate (Υ_e) is greater than secrecy capacity (C_s), where $C_s = [\log_2(1+\gamma_{f,j}) - \log_2(1+\gamma_{e,j})]^+$ and $[z]^+ = \max\{z, 0\}$. So, mathematically, SOP can be described as [49, Eq. (14)]

$$\begin{aligned} SOP &= \Pr\{C_s(\gamma_{f,j}, \gamma_{e,j}) \leq \Upsilon_e\} \\ &= \int_0^\infty F_{\gamma_{f,j}}(\sigma\gamma + \sigma - 1) f_{\gamma_{e,j}}(\gamma) d\gamma, \end{aligned} \tag{30}$$

where $\sigma = 2^{\Upsilon_e}$ and $\Upsilon_e > 0$. Since Meijer's G function exists in (21) and (29), derivation of SOP utilizing (30) is almost impossible. Hence, the lower bound of SOP can be derived as [50], [51]

$$SOP \geq SOP_L = \int_0^\infty F_{\gamma_{f,j}}(\sigma\gamma) f_{\gamma_{e,j}}(\gamma) d\gamma. \tag{31}$$

1) Scenario I: Substituting (21) and (8) into (31), SOP is written as

$$\begin{aligned} SOP_L^I = \frac{\alpha_e \delta_e^{\mu_e} P_o}{2\Gamma(\mu_e)} \Im_1 + (1 - P_o) K \varsigma_n \\ \times \sum_{m_o=0}^{\beta_o} \left\{ \frac{\alpha_e \delta_e^{\mu_e}}{2\Gamma(\mu_e)} \Im_2 - \Xi_5^I \Im_4 \right\} - P_o \sum_{m_r=0}^{\mu_r - 1} \Xi_5^I \Im_3, \end{aligned} \tag{32}$$

where $\Xi_5^I = \binom{\Xi_2^I + m_2 - 1}{m_2} \frac{\alpha_p \delta_p^{\mu_p}}{2\Gamma(\mu_p)} \frac{\alpha_e \delta_e^{\mu_e}}{2\Gamma(\mu_e)} \frac{\delta_r^{m_r}}{m_r!} \frac{\Gamma(\Xi_2^I)}{\tilde{\alpha_p}} (\frac{\sigma}{\Psi_Q})^{\tilde{\alpha_r} m_r} (-1)^{m_2} (\Xi_1^I \sigma^{\tilde{\alpha_r}})^{m_2} (\Phi_p^{-\tilde{\alpha_p}})^{-\Xi_2^I - m_2}$ and the four integral terms, $\Im_1$, $\Im_2$, $\Im_3$, and $\Im_4$ are derived as follows.

Derivation of $\Im_1$*:* Utilizing the formula of [42, Eq. (3.326.2)], $\Im_1$ is expressed as

$$\Im_1 = \int_0^\infty e^{-\delta_e \gamma^{\tilde{\alpha_e}}} \gamma^{\Theta_e} d\gamma = \frac{\Gamma\left(\frac{\Theta_e + 1}{\tilde{\alpha_e}}\right)}{\tilde{\alpha_e}} \delta_e^{-\frac{\Theta_e + 1}{\tilde{\alpha_e}}}. \tag{33}$$

Derivation of $\Im_2$*:* $\Im_2$ is written as

$$\Im_2 = \int_0^\infty e^{-\delta_e \gamma^{\tilde{\alpha_e}}} \gamma^{\Theta_e} G_{s+1,3\,s+1}^{3\,s,1} \left[\frac{V\sigma\gamma}{\mu_s} \middle| \begin{matrix} 1, q_1 \\ q_2, 0 \end{matrix} \right] d\gamma. \tag{34}$$

Now, with the help of [46, Eqs. (2.24.1.1) and (8.4.3.1)], $\Im_2$ is converted as

$$\begin{aligned} \Im_2 &= \int_0^\infty \gamma^{\Theta_e} G_{0,1}^{1,0} \left[\delta_e \gamma^{\tilde{\alpha_e}} \middle| \begin{matrix} - \\ 0 \end{matrix} \right] G_{s+1,3\,s+1}^{3\,s,1} \left[\frac{V\sigma\gamma}{\mu_s} \middle| \begin{matrix} 1, q_1 \\ q_2, 0 \end{matrix} \right] d\gamma \\ &= \frac{\tilde{\alpha_e}^{s(2\Theta_e+1)} \left(\frac{V\sigma}{\mu_s}\right)^{-(\Theta_e+1)}}{(2\pi)^{s(\tilde{\alpha_e}-1)}} \\ &\quad \times G_{\tilde{\alpha_e}(3\,s+1),1+\tilde{\alpha_e}(s+1)}^{1+\tilde{\alpha_e},3\,s\tilde{\alpha_e}} \left[\frac{\delta_e \tilde{\alpha_e}^{2\,s\tilde{\alpha_e}}}{\left(\frac{V\sigma}{\mu_s}\right)^{\tilde{\alpha_e}}} \middle| \begin{matrix} \zeta_1, \Delta(\tilde{\alpha_e}, -\Theta_e) \\ 0, \zeta_2, \zeta_3 \end{matrix} \right], \end{aligned} \tag{35}$$

$$\begin{aligned} F_{\gamma_{r,II}}(\gamma) = 1 + \Xi_5^{II} - \sum_{m_p=0}^{\mu_p-1} \Xi_1^{II} - \sum_{m_r=0}^{\mu_r-1} \Xi_2^{II} \gamma^{\tilde{\alpha_r} m_r} e^{-\delta_r \Psi_T^{-\tilde{\alpha_r}} \gamma^{\tilde{\alpha_r}}} + \sum_{m_p=0}^{\mu_p-1} \sum_{m_r=0}^{\mu_r-1} \Xi_3^{II} \gamma^{\tilde{\alpha_r} m_r} e^{-(\delta_p \Psi_Q^{\tilde{\alpha_p}} \Psi_T^{-\tilde{\alpha_p}} + \delta_r \Psi_T^{-\tilde{\alpha_r}} \gamma^{\tilde{\alpha_r}})} \\ - \sum_{m_r=0}^{\mu_r-1} \sum_{m_3=0}^{\Omega-1} \sum_{m_4=0}^{m_3} \sum_{m_5=0}^{\infty} \binom{m_3}{m_4} \binom{\Omega + m_5 - 1}{m_5} \Xi_6^{II} \gamma^{\tilde{\alpha_r}(m_r+m_4+m_5)} e^{-(\delta_p \Psi_Q^{\tilde{\alpha_r}} \Psi_T^{-\tilde{\alpha_r}} + \delta_r \Psi_T^{-2\tilde{\alpha_r}} \Psi_Q^{\tilde{\alpha_r}} \gamma^{\tilde{\alpha_r}})}. \end{aligned} \tag{27}$$

$$\begin{aligned} F_{\gamma_{f,II}}(\gamma) = P_o \Bigg\{ \mathcal{X} - \sum_{m_r=0}^{\mu_r-1} \Xi_2^{II} \gamma^{\tilde{\alpha_r} m_r} e^{-\delta_r \Psi_T^{-\tilde{\alpha_r}} \gamma^{\tilde{\alpha_r}}} + \sum_{m_p=0}^{\mu_p-1} \sum_{m_r=0}^{\mu_r-1} \Xi_3^{II} \gamma^{\tilde{\alpha_r} m_r} e^{-(\delta_p \Psi_Q^{\tilde{\alpha_p}} \Psi_T^{-\tilde{\alpha_p}} + \delta_r \Psi_T^{-\tilde{\alpha_r}} \gamma^{\tilde{\alpha_r}})} - \sum_{m_r=0}^{\mu_r-1} \sum_{m_3=0}^{\Omega-1} \\ \times \sum_{m_4=0}^{m_3} \sum_{m_5=0}^{\infty} \binom{m_3}{m_4} \binom{\Omega + m_5 - 1}{m_5} \Xi_6^{II} \gamma^{\tilde{\alpha_r}(m_r+m_4+m_5)} e^{-(\delta_p \Psi_Q^{\tilde{\alpha_r}} \Psi_T^{-\tilde{\alpha_r}} + \delta_r \Psi_T^{-2\tilde{\alpha_r}} \Psi_Q^{\tilde{\alpha_r}} \gamma^{\tilde{\alpha_r}})} \Bigg\} + (1 - P_o) K \sum_{m_o=0}^{\beta_o} \varsigma_n \\ \times G_{s+1,3\,s+1}^{3\,s,1} \left[\frac{V\gamma}{\mu_s} \middle| \begin{matrix} 1, q_1 \\ q_2, 0 \end{matrix} \right] \Bigg\{ \mathcal{X} - \sum_{m_r=0}^{\mu_r-1} \Xi_2^{II} \gamma^{\tilde{\alpha_r} m_r} e^{-\delta_r \Psi_T^{-\tilde{\alpha_r}} \gamma^{\tilde{\alpha_r}}} + \sum_{m_p=0}^{\mu_p-1} \sum_{m_r=0}^{\mu_r-1} \Xi_3^{II} \gamma^{\tilde{\alpha_r} m_r} e^{-(\delta_p \Psi_Q^{\tilde{\alpha_p}} \Psi_T^{-\tilde{\alpha_p}} + \delta_r \Psi_T^{-\tilde{\alpha_r}} \gamma^{\tilde{\alpha_r}})} \\ - \sum_{m_r=0}^{\mu_r-1} \sum_{m_3=0}^{\Omega-1} \sum_{m_4=0}^{m_3} \sum_{m_5=0}^{\infty} \binom{m_3}{m_4} \binom{\Omega + m_5 - 1}{m_5} \Xi_6^{II} \gamma^{\tilde{\alpha_r}(m_r+m_4+m_5)} e^{-(\delta_p \Psi_Q^{\tilde{\alpha_r}} \Psi_T^{-\tilde{\alpha_r}} + \delta_r \Psi_T^{-2\tilde{\alpha_r}} \Psi_Q^{\tilde{\alpha_r}} \gamma^{\tilde{\alpha_r}})} \Bigg\}. \end{aligned} \tag{29}$$

where $\zeta_1=\Delta(\tilde{\alpha_e},-\Theta_e-q_2)$, $\zeta_2=\Delta(\tilde{\alpha_e},-\Theta_e-1)$, $\zeta_3=\Delta(\tilde{\alpha_e},-\Theta_e-q_1)$, and $\Delta(c,r)=\frac{r}{c},\frac{r+1}{c},\ldots,\frac{r+c-1}{c}$ as defined in [52, Eq. (22)].

Derivation of $\Im_3$*:* $\Im_3$ is expressed as

$$\Im_3=\int_0^{\infty}(\Xi_1^I\sigma^{\tilde{\alpha_r}}\gamma^{\tilde{\alpha_p}}+\Phi_p^{-\tilde{\alpha_p}})^{-\Xi_2^I}\gamma^{\Theta_e+\tilde{\alpha_r}m_r}e^{-\delta_e\gamma^{\tilde{\alpha_e}}}d\gamma. \tag{36}$$

Utilizing binomial expansion and [42, Eq. (3.326.2)], $\Im_3$ is expressed in alternative form as

$$\Im_3=\sum_{m_2=0}^{\infty}\int_0^{\infty}\gamma^{\Xi_3^I}e^{-\delta_e\gamma^{\tilde{\alpha_e}}}d\gamma=\sum_{m_2=0}^{\infty}\frac{\Gamma(\Xi_4^I)}{\tilde{\alpha_e}}\delta_e^{-\Xi_4^I}, \tag{37}$$

where $\Xi_3^I=\Theta_e+\tilde{\alpha_r}m_r+\tilde{\alpha_p}m_2$ and $\Xi_4^I=\frac{\Xi_3^I+1}{\tilde{\alpha_e}}$.

Derivation of $\Im_4$*:* Following the similar approach of $\Im_2$ and $\Im_3$, $\Im_4$ is illustrated as

$$\begin{aligned}\Im_4&=\sum_{m_2=0}^{\infty}\int_0^{\infty}e^{-\delta_e\gamma^{\tilde{\alpha_e}}}\gamma^{\Xi_3^I}G_{s+1,3\,s+1}^{3\,s,1}\left[\frac{V\sigma\gamma}{\mu_s}\middle|\begin{matrix}1,q_1\\q_2,0\end{matrix}\right]d\gamma\\&=\sum_{m_2=0}^{\infty}\frac{\tilde{\alpha_e}^{s(2\,\Xi_3^I+1)}\left(\frac{V\sigma}{\mu_s}\right)^{-(\Xi_3^I+1)}}{(2\pi)^{s(\tilde{\alpha_e}-1)}}\\&\quad\times G_{\tilde{\alpha_e}(3\,s+1),1+\tilde{\alpha_e}(s+1)}^{1+\tilde{\alpha_e},3\,s\tilde{\alpha_e}}\left[\frac{\delta_e\tilde{\alpha_e}^{2\,s\tilde{\alpha_e}}}{\left(\frac{V\sigma}{\mu_s}\right)^{\tilde{\alpha_e}}}\middle|\begin{matrix}\zeta_4,\Delta(\tilde{\alpha_e},-\Xi_3^I)\\0,\zeta_5,\zeta_6\end{matrix}\right].\end{aligned} \tag{38}$$

where $\zeta_4=\Delta(\tilde{\alpha_e},-\Xi_3^I-q_2)$, $\zeta_5=\Delta(\tilde{\alpha_e},-\Xi_3^I-1)$, and $\zeta_6=\Delta(\tilde{\alpha_e},-\Xi_3^I-q_1)$.

2) Scenario II: Substituting (8) and (29) into (31), SOP for double power constraints scenario is derived as (39) shown at the bottom of next page, where the eight integral terms, $\mathcal{R}_1$, $\mathcal{R}_2$, $\mathcal{R}_3$, $\mathcal{R}_4$, $\mathcal{R}_5$, $\mathcal{R}_6$, $\mathcal{R}_7$, and $\mathcal{R}_8$ are derived as follows.

Derivation of $\mathcal{R}_1$*:* Utilizing [42, Eq. (3.326.2)], $\mathcal{R}_1$ is expressed as

$$\mathcal{R}_1=\int_0^{\infty}e^{-\delta_e\gamma^{\tilde{\alpha_e}}}\gamma^{\Theta_e}d\gamma=\frac{\Gamma\left(\frac{\Theta_e+1}{\tilde{\alpha_e}}\right)}{\tilde{\alpha_e}}\delta_e^{-\frac{\Theta_e+1}{\tilde{\alpha_e}}}. \tag{40}$$

Derivation of $\mathcal{R}_2$ *and* $\mathcal{R}_3$*:* $\mathcal{R}_2$ and $\mathcal{R}_3$ are expressed as

$$\mathcal{R}_2=\mathcal{R}_3=\int_0^{\infty}\gamma^{\tilde{\alpha_r}m_r+\Theta_e}e^{-\delta_r\sigma^{\tilde{\alpha_r}}\Psi_T^{-\tilde{\alpha_r}}\gamma^{\tilde{\alpha_r}}}e^{-\delta_e\gamma^{\tilde{\alpha_e}}}d\gamma. \tag{41}$$

Following some mathematical manipulations defined in [53] and utilizing identities [46, Eqs. (8.4.3.1) and (2.24.1.1)], $\mathcal{R}_2$ and $\mathcal{R}_3$ are further derived as

$$\begin{aligned}\mathcal{R}_2=\mathcal{R}_3&=\int_0^{\infty}\gamma^{\frac{\tilde{\alpha_r}m_r+\Theta_e}{\tilde{\alpha_r}}}e^{-\delta_r\Psi_T^{-\tilde{\alpha_r}}\sigma^{\tilde{\alpha_r}}\gamma}e^{-\delta_e\gamma^{\frac{\tilde{\alpha_e}}{\tilde{\alpha_r}}}}d\left(\gamma^{\frac{1}{\tilde{\alpha_r}}}\right)\\&=\frac{1}{\tilde{\alpha_r}}\int_0^{\infty}\gamma^{\Xi_7^{II}-1}e^{-\delta_r\Psi_T^{-\tilde{\alpha_r}}\sigma^{\tilde{\alpha_r}}\gamma}e^{-\delta_e\gamma^{\frac{\tilde{\alpha_e}}{\tilde{\alpha_r}}}}d\gamma\\&=\frac{1}{\tilde{\alpha_r}}\int_0^{\infty}\gamma^{\Xi_7^{II}-1}G_{0,1}^{1,0}\left[\delta_r\Psi_T^{-\tilde{\alpha_r}}\sigma^{\tilde{\alpha_r}}\gamma\middle|\begin{matrix}-\\0\end{matrix}\right]\\&\quad\times G_{0,1}^{1,0}\left[\delta_e\gamma^{\frac{\tilde{\alpha_e}}{\tilde{\alpha_r}}}\middle|\begin{matrix}-\\0\end{matrix}\right]d\gamma=\frac{\tilde{\alpha_e}^{\Xi_7^{II}-\frac{1}{2}}(\delta_r\Psi_T^{-\tilde{\alpha_r}}\sigma^{\tilde{\alpha_r}})^{-\Xi_7^{II}}}{\tilde{\alpha_r}^{\frac{1}{2}}(2\pi)^{\frac{1}{2}(\tilde{\alpha_e}+\tilde{\alpha_r}-2)}}\\&\quad\times G_{\tilde{\alpha_e},\tilde{\alpha_r}}^{\tilde{\alpha_r},\tilde{\alpha_e}}\left[\frac{\delta_e^{\tilde{\alpha_r}}\tilde{\alpha_r}^{-\tilde{\alpha_r}}}{(\delta_r\Psi_T^{-\tilde{\alpha_r}}\sigma^{\tilde{\alpha_r}})^{\tilde{\alpha_e}}\tilde{\alpha_e}^{-\tilde{\alpha_e}}}\middle|\begin{matrix}\Delta(\tilde{\alpha_e},1-\Xi_7^{II})\\0\end{matrix}\right],\end{aligned} \tag{42}$$

where $\Xi_7^{II}=\frac{\tilde{\alpha_r}m_r+\Theta_e+\tilde{\alpha_r}}{\tilde{\alpha_r}}$.

Derivation of $\mathcal{R}_4$*:* By following the similar approach as of $\mathcal{R}_2$ and $\mathcal{R}_3$, $\mathcal{R}_4$ is expressed as

$$\begin{aligned}\mathcal{R}_4&=\int_0^{\infty}\gamma^{\tilde{\alpha_r}(m_r+m_4+m_5)+\Theta_e}e^{-\delta_r\Psi_T^{-2\tilde{\alpha_r}}\Psi_Q^{\tilde{\alpha_r}}\sigma^{\tilde{\alpha_r}}\gamma^{\tilde{\alpha_r}}}e^{-\delta_e\gamma^{\tilde{\alpha_e}}}d\gamma\\&=\int_0^{\infty}\gamma^{\frac{\tilde{\alpha_r}(m_r+m_4+m_5)+\Theta_e}{\tilde{\alpha_r}}}e^{-\delta_r\Psi_T^{-2\tilde{\alpha_r}}\Psi_Q^{\tilde{\alpha_r}}\sigma^{\tilde{\alpha_r}}\gamma}e^{-\delta_e\gamma^{\frac{\tilde{\alpha_e}}{\tilde{\alpha_r}}}}d\left(\gamma^{\frac{1}{\tilde{\alpha_r}}}\right)\\&=\frac{1}{\tilde{\alpha_r}}\int_0^{\infty}\gamma^{\Xi_8^{II}-1}e^{-\delta_r\Psi_T^{-2\tilde{\alpha_r}}\Psi_Q^{\tilde{\alpha_r}}\sigma^{\tilde{\alpha_r}}\gamma}e^{-\delta_e\gamma^{\frac{\tilde{\alpha_e}}{\tilde{\alpha_r}}}}d\gamma\\&=\frac{1}{\tilde{\alpha_r}}\int_0^{\infty}\gamma^{\Xi_8^{II}-1}G_{0,1}^{1,0}\left[\delta_r\Psi_T^{-2\tilde{\alpha_r}}\Psi_Q^{\tilde{\alpha_r}}\sigma^{\tilde{\alpha_r}}\gamma\middle|\begin{matrix}-\\0\end{matrix}\right]\\&\quad\times G_{0,1}^{1,0}\left[\delta_e\gamma^{\frac{\tilde{\alpha_e}}{\tilde{\alpha_r}}}\middle|\begin{matrix}-\\0\end{matrix}\right]d\gamma=\frac{\tilde{\alpha_e}^{\Xi_8^{II}-\frac{1}{2}}(\delta_r\Psi_T^{-2\tilde{\alpha_r}}\Psi_Q^{\tilde{\alpha_r}}\sigma^{\tilde{\alpha_r}})^{-\Xi_8^{II}}}{\tilde{\alpha_r}^{\frac{1}{2}}(2\pi)^{\frac{1}{2}(\tilde{\alpha_e}+\tilde{\alpha_r}-2)}}\\&\quad\times G_{\tilde{\alpha_e},\tilde{\alpha_r}}^{\tilde{\alpha_r},\tilde{\alpha_e}}\left[\frac{\delta_e^{\tilde{\alpha_r}}\tilde{\alpha_r}^{-\tilde{\alpha_r}}}{(\delta_r\Psi_T^{-2\tilde{\alpha_r}}\Psi_Q^{\tilde{\alpha_r}}\sigma^{\tilde{\alpha_r}})^{\tilde{\alpha_e}}\tilde{\alpha_e}^{-\tilde{\alpha_e}}}\middle|\begin{matrix}\Delta(\tilde{\alpha_e},1-\Xi_8^{II})\\0\end{matrix}\right],\end{aligned} \tag{43}$$

where $\Xi_8^{II}=\frac{\tilde{\alpha_r}(m_r+m_4+m_5)+\Theta_e+\tilde{\alpha_r}}{\tilde{\alpha_r}}$.

Derivation of $\mathcal{R}_5$*:* With some mathematical manipulations and following identities [46, Eqs. (8.4.3.1) and (2.24.1.1)], $\mathcal{R}_5$

$$\begin{aligned}SOP_L^{II}=\frac{\alpha_e\delta_e^{\mu_e}}{2\Gamma(\mu_e)}\Bigg[P_o\Bigg\{&\mathcal{X}\mathcal{R}_1-\sum_{m_r=0}^{\mu_r-1}\Xi_2^{II}\sigma^{\tilde{\alpha_r}m_r}\mathcal{R}_2+\sum_{m_p=0}^{\mu_p-1}\sum_{m_r=0}^{\mu_r-1}\Xi_3^{II}\sigma^{\tilde{\alpha_r}m_r}e^{-\delta_p\Psi_Q^{\tilde{\alpha_p}}\Psi_T^{-\tilde{\alpha_p}}}\mathcal{R}_3-\sum_{m_r=0}^{\mu_r-1}\sum_{m_3=0}^{\Omega-1}\sum_{m_4=0}^{m_3}\sum_{m_5=0}^{\infty}\\&\times\binom{\Omega+m_5-1}{m_5}\binom{m_3}{m_4}\Xi_6^{II}\sigma^{\tilde{\alpha_r}(m_r+m_4+m_5)}e^{-\delta_p\Psi_Q^{\tilde{\alpha_r}}\Psi_T^{-\tilde{\alpha_r}}}\mathcal{R}_4\Bigg\}+(1-P_o)K\sum_{m_o=0}^{\beta_o}\varsigma_n\Bigg\{\mathcal{X}\mathcal{R}_5-\sum_{m_r=0}^{\mu_r-1}\Xi_2^{II}\mathcal{R}_6\,\sigma^{\tilde{\alpha_r}m_r}+\sum_{m_p=0}^{\mu_p-1}\\&\times\sum_{m_r=0}^{\mu_r-1}\Xi_3^{II}\mathcal{R}_7\sigma^{\tilde{\alpha_r}m_r}e^{-\delta_p\Psi_Q^{\tilde{\alpha_p}}\Psi_T^{-\tilde{\alpha_p}}}-\sum_{m_r=0}^{\mu_r-1}\sum_{m_3=0}^{\Omega-1}\sum_{m_4=0}^{m_3}\sum_{m_5=0}^{\infty}\binom{m_3}{m_4}\binom{\Omega+m_5-1}{m_5}\Xi_6^{II}\mathcal{R}_8\,\sigma^{\tilde{\alpha_r}(m_r+m_4+m_5)}e^{-\delta_p\Psi_Q^{\tilde{\alpha_r}}\Psi_T^{-\tilde{\alpha_r}}}\Bigg\}\Bigg].\end{aligned} \tag{39}$$

is derived as

$$\mathcal{R}_5 = \int_0^\infty \gamma^{\Theta_e} e^{-\delta_e \gamma^{\tilde{\alpha_e}}} G_{s+1,3\,s+1}^{3\,s,1}\left[\frac{V\sigma\gamma}{\mu_s}\middle|\begin{matrix}1, q_1\\ q_2, 0\end{matrix}\right] d\gamma$$
$$= \int_0^\infty \gamma^{\Theta_e} G_{0,1}^{1,0}\left[\delta_e\gamma^{\tilde{\alpha_e}}\middle|\begin{matrix}-\\ 0\end{matrix}\right] G_{s+1,3\,s+1}^{3\,s,1}\left[\frac{V\sigma\gamma}{\mu_s}\middle|\begin{matrix}1, q_1\\ q_2, 0\end{matrix}\right] d\gamma$$
$$= \frac{\tilde{\alpha_e}^{\,s(2\Theta_e+1)}\left(\frac{V\sigma}{\mu_s}\right)^{-(\Theta_e+1)}}{(2\pi)^{s(\tilde{\alpha_e}-1)}}$$
$$\times G_{\tilde{\alpha_e}(3\,s+1),1+\tilde{\alpha_e}(s+1)}^{1+\tilde{\alpha_e},3\,s\tilde{\alpha_e}}\left[\frac{\delta_e\tilde{\alpha_e}^{\,2\,s\tilde{\alpha_e}}}{\left(\frac{V\sigma}{\mu_s}\right)^{\tilde{\alpha_e}}}\middle|\begin{matrix}\zeta_1, \Delta(\tilde{\alpha_e}, -\Theta_e)\\ 0, \zeta_2, \zeta_3\end{matrix}\right]. \tag{44}$$

Derivation of $\mathcal{R}_6$ and $\mathcal{R}_7$: $\mathcal{R}_6$ and $\mathcal{R}_7$ are derived by following [46, Eq. (8.4.3.1)] as

$$\mathcal{R}_6 = \mathcal{R}_7 = \int_0^\infty \gamma^{\tilde{\alpha_r} m_r + \Theta_e} e^{-\delta_r \Psi_T^{-\tilde{\alpha_r}} \sigma^{\tilde{\alpha_r}} \gamma^{\tilde{\alpha_r}}} e^{-\delta_e \gamma^{\tilde{\alpha_e}}}$$
$$\times G_{s+1,3\,s+1}^{3\,s,1}\left[\frac{V\sigma\gamma}{\mu_s}\middle|\begin{matrix}1, q_1\\ q_2, 0\end{matrix}\right] d\gamma$$
$$= \int_0^\infty \gamma^{\tilde{\alpha_r} m_r + \Theta_e} G_{0,1}^{1,0}\left[\delta_r \Psi_T^{-\tilde{\alpha_r}} \sigma^{\tilde{\alpha_r}} \gamma^{\tilde{\alpha_r}}\middle|\begin{matrix}-\\ 0\end{matrix}\right]$$
$$\times G_{0,1}^{1,0}\left[\delta_e\gamma^{\tilde{\alpha_e}}\middle|\begin{matrix}-\\ 0\end{matrix}\right] G_{s+1,3\,s+1}^{3\,s,1}\left[\frac{V\sigma\gamma}{\mu_s}\middle|\begin{matrix}1, q_1\\ q_2, 0\end{matrix}\right] d\gamma. \tag{45}$$

Now, for tractable analysis, transforming Meijer's G functions into Fox's H functions via utilizing [54, Eqs. (6.2.3) and (6.2.8)] and performing integration by means of [55, Eq. (2.3)] and [39, Eq. (3)], $\mathcal{R}_6$ and $\mathcal{R}_7$ are obtained as

$$\mathcal{R}_6 = \mathcal{R}_7 = \int_0^\infty \gamma^{\tilde{\alpha_r} m_r + \Theta_e} H_{s+1,3\,s+1}^{3\,s,1}\left[\frac{V\sigma\gamma}{\mu_s}\middle|\begin{matrix}(1,1),(q_1,1)\\ (q_2,1),(0,1)\end{matrix}\right]$$
$$\times H_{0,1}^{1,0}\left[\Xi_{10}^{II}\gamma^{\tilde{\alpha_r}}\middle|\begin{matrix}-\\ (0,1)\end{matrix}\right] H_{0,1}^{1,0}\left[\delta_e\gamma^{\tilde{\alpha_e}}\middle|\begin{matrix}-\\ (0,1)\end{matrix}\right] d\gamma = \frac{\delta_e^{-\frac{\Xi_9^{II}}{\tilde{\alpha_e}}}}{\tilde{\alpha_e}}$$
$$\times H_{1,0:0,1:s+1,3\,s+1}^{1,0:1,0:3\,s,1}\left[\begin{matrix}J_1\\ J_2\end{matrix}\middle|\begin{matrix}-\\ (0,1)\end{matrix}\middle|\begin{matrix}(1,1),(q_1,1)\\ (q_2,1),(0,1)\end{matrix}\middle|J_3, J_4\right], \tag{46}$$

where $\Xi_9^{II} = \tilde{\alpha_r} m_r + \Theta_e + 1$, $\Xi_{10}^{II} = \delta_r \Psi_T^{-\tilde{\alpha_r}} \sigma^{\tilde{\alpha_r}}$, $J_1 = (1 - \frac{\Xi_9^{II}}{\tilde{\alpha_e}}; \frac{\tilde{\alpha_r}}{\tilde{\alpha_e}}, \frac{1}{\tilde{\alpha_e}})$, $J_2 = (1; -)$, $J_3 = \Xi_{10}^{II}\delta_e^{-\frac{\tilde{\alpha_r}}{\tilde{\alpha_e}}}$, $J_4 = V\sigma\mu_s^{-1}\delta_e^{-\frac{1}{\tilde{\alpha_e}}}$, and $H_{p,q}^{m,n}[\cdot]$ is the Fox's H function introduced in [56, Eq. (1.2)], and $H_{c_1,d_1:c_2,d_2:c_3,d_3}^{x_1,y_1:x_2,y_2:x_3,y_3}[\cdot]$ is the extended generalized bivariate Fox's H function (EGBFHF) as explained in [56, Eq. (2.57)].

Derivation of $\mathcal{R}_8$: $\mathcal{R}_8$ is derived by following the similar identities from $\mathcal{R}_6$ and $\mathcal{R}_7$ as

$$\mathcal{R}_8 = \int_0^\infty \gamma^{\tilde{\alpha_r}(m_r+m_4+m_5)+\Theta_e} e^{-\delta_r \Psi_T^{-2\tilde{\alpha_r}} \Psi_Q^{\tilde{\alpha_r}} \sigma^{\tilde{\alpha_r}} \gamma^{\tilde{\alpha_r}}} e^{-\delta_e \gamma^{\tilde{\alpha_e}}}$$
$$\times G_{s+1,3\,s+1}^{3\,s,1}\left[\frac{V\sigma\gamma}{\mu_s}\middle|\begin{matrix}1, q_1\\ q_2, 0\end{matrix}\right] d\gamma = \int_0^\infty \gamma^{\tilde{\alpha_r}(m_r+m_4+m_5)+\Theta_e}$$
$$\times G_{0,1}^{1,0}\left[\Xi_{12}^{II}\gamma^{\tilde{\alpha_r}}\middle|\begin{matrix}-\\ 0\end{matrix}\right] G_{0,1}^{1,0}\left[\delta_e\gamma^{\tilde{\alpha_e}}\middle|\begin{matrix}-\\ 0\end{matrix}\right]$$
$$\times G_{s+1,3\,s+1}^{3\,s,1}\left[\frac{V\sigma\gamma}{\mu_s}\middle|\begin{matrix}1, q_1\\ q_2, 0\end{matrix}\right] d\gamma = \tilde{\alpha_e}^{-1}\delta_e^{-\frac{\Xi_{11}^{II}}{\tilde{\alpha_e}}}$$
$$\times H_{1,0:0,1:s+1,3\,s+1}^{1,0:1,0:3\,s,1}\left[\begin{matrix}J_5\\ J_2\end{matrix}\middle|\begin{matrix}-\\ (0,1)\end{matrix}\middle|\begin{matrix}(1,1),(q_1,1)\\ (q_2,1),(0,1)\end{matrix}\middle|J_6, J_4\right], \tag{47}$$

where $\Xi_{11}^{II} = \tilde{\alpha_r}(m_r + m_4 + m_5) + \Theta_e + 1$, $\Xi_{12}^{II} = \delta_r \Psi_T^{-2\tilde{\alpha_r}} \Psi_Q^{\tilde{\alpha_r}} \sigma^{\tilde{\alpha_r}}$, $J_5 = (1 - \frac{\Xi_{11}^{II}}{\tilde{\alpha_e}}; \frac{\tilde{\alpha_r}}{\tilde{\alpha_e}}, \frac{1}{\tilde{\alpha_e}})$, and $J_6 = \Xi_{12}^{II}\,\delta_e^{-\frac{\tilde{\alpha_r}}{\tilde{\alpha_e}}}$.

B. Strictly Positive Secrecy Capacity Analysis

In order to ensure secrecy in a wiretap-prone model, the probability of SPSC acts as one of the crucial performance metrics that ensure uninterrupted data stream conveyance only when the secrecy behavior of the system remains up to scratch ($\gamma_{f,j} > \gamma_{e,j}$). Mathematically, the analytical expression of the probability of SPSC can be easily deducted from the SOP that is given as [32, Eq. (25)]

$$SPSC = \Pr\{C_s > 0\}$$
$$= 1 - \Pr\{C_s \le 0\}.$$
$$\text{Hence, } SPSC^I = 1 - \text{SOP}_L^I|_{\Upsilon_e=0}, \text{ (Scenario-I)} \tag{48}$$
$$\text{and } SPSC^{II} = 1 - \text{SOP}_L^{II}|_{\Upsilon_e=0}. \text{ (Scenario-II)} \tag{49}$$

C. Effective Secrecy Throughput Analysis

EST is another secrecy performance metric that ensures achievable secure average throughput measurements. When the reliability issue is considered equally important along with the security issue then this parameter is considered. Mathematically, EST is formulated as the product of target secrecy rate and the probability of successful transmission that is given as [57, Eq. (5)]

$$EST = \Upsilon_e(1 - SOP).$$
$$\text{Hence, } EST^I = \Upsilon_e(1 - SOP_L^I), \text{ (Scenario-I)} \tag{50}$$
$$\text{and } EST^{II} = \Upsilon_e(1 - SOP_L^{II}). \text{ (Scenario-II)} \tag{51}$$

VI. Numerical Results

In this section, the impacts of all the system parameters (e.g., α_i, μ_i, Φ_i, Ψ_Q, Ψ_T, P_o, α_o, β_o, ϵ, and s) on the secrecy behavior of the proposed scenarios are illustrated graphically utilizing the expressions in (32), (39), (48), (49), (50), and (51). Note that the univariate Meijer's G and Fox's H functions can be easily computed utilizing standard Mathematica packages whereas the EGBFHF is computed utilizing [39, Table I]. Moreover, all the mathematical expressions are also validated via MC simulations averaging 10^6 random samples of $\alpha - \mu$ and Málaga random variables. It can clearly be seen that MC simulation results are in good agreement with the analytical results that strongly

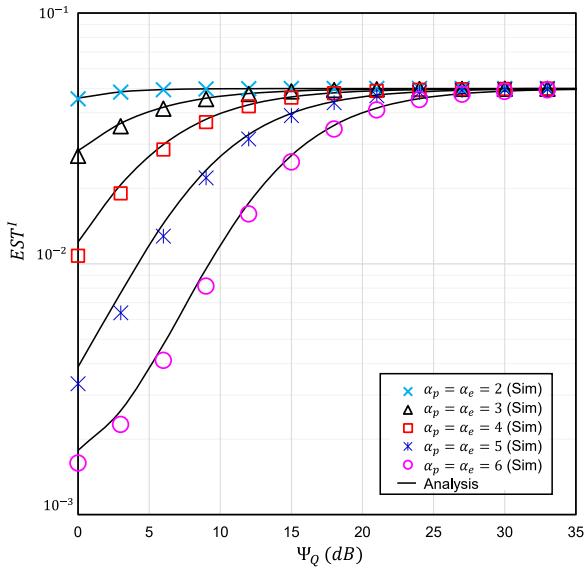

Fig. 2. The EST versus Ψ_Q for selected values of α_p and α_e with $\alpha_o = 2.296$, $\beta_o = 2$, $\Omega_o = 1$, $g = 2$, $s = 2$, $\epsilon = 1$, $P_o = 0.5$, $\alpha_r = 2$, $\mu_r = \mu_p = \mu_e = 2$, $\Phi_r = 15\,dB$, $\Phi_p = 10\,dB$, $\Phi_e = \mu_s - 5\,dB$, and $\Upsilon_e = 0.05$ bits/sec/Hz.

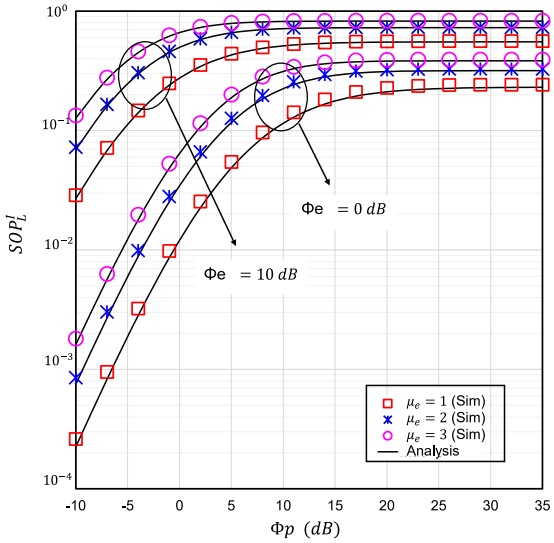

Fig. 4. The SOP versus Φ_p for selected values of μ_e and Φ_e with $\alpha_o = 2.296$, $\beta_o = 2$, $\Omega_o = 1$, $g = 2$, $s = 1$, $\epsilon = 1$, $\alpha_r = \alpha_p = \alpha_e = 2$, $\mu_r = \mu_p = 2$, $P_o = 0.1$, $\Phi_r = 15\,dB$, $\mu_r = 12\,dB$, $\Psi_Q = -5\,dB$, and $\Upsilon_e = 0.05$ bits/sec/Hz.

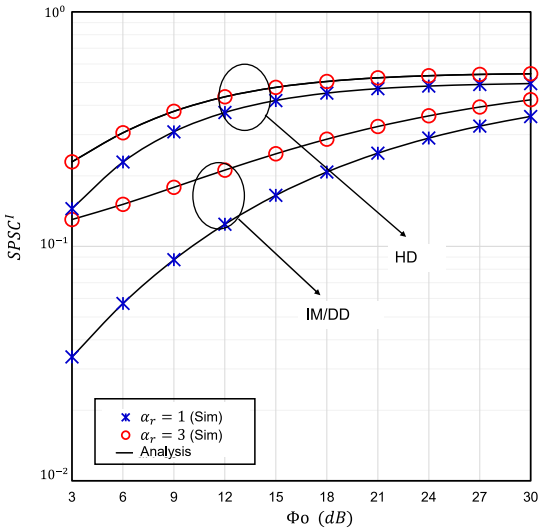

Fig. 3. The SPSC versus Φ_o for selected values of α_r and s with $\alpha_o = 2.296$, $\beta_o = 2, \Omega_o = 1, g = 2, \epsilon = 1, P_o = 0.5, \alpha_p = \alpha_e = 5, \mu_r = \mu_p = \mu_e = 6$, $\Phi_r = \Phi_p = 15\,dB$, $\Phi_e = 0\,dB$, and $\Psi_Q = 15\,dB$.

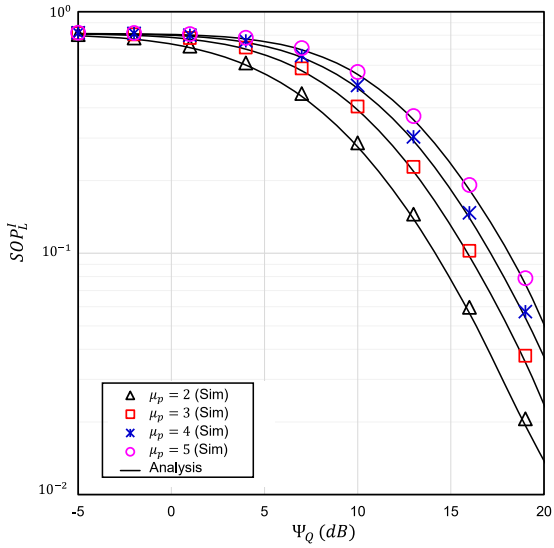

Fig. 5. The SOP versus Ψ_Q for selected values of μ_p with $\alpha_o = 2.296$, $\beta_o = 2$, $\Omega_o = 1$, $g = 2$, $\epsilon = 1$, $s = 1$, $\alpha_r = \alpha_p = \alpha_e = 2$, $\mu_r = \mu_e = 2$, $P_o = 0.1$, $\Phi_p = 10\,dB$, $\Phi_r = 15\,dB$ $\Phi_o = 10\,dB$, $\Phi_e = 10\,dB$, and $\Upsilon_e = 0.05$ bits/sec/Hz.

corroborate the analysis of this paper. According to [43], all the numerical results due to the FSO link, are demonstrated assuming $(\alpha_o, \beta_o) = (2.296, 2)$ for strong, $(\alpha_o, \beta_o) = (4.2, 3)$ for moderate, and $(\alpha_o, \beta_o) = (8, 4)$ for weak turbulences, $r = 1$ for HD and $r = 2$ for IM/DD techniques. On the other hand, similar to [5], we assume that RF links have the following parameters: $\alpha_r = \alpha_p = \alpha_e$, $\mu_r = \mu_p = \mu_e$, and $\Upsilon_e = 0.05$ bits/sec/Hz, unless specified otherwise. Note that even though the representation of (27) and (29) are done through an infinite series, it quickly leads to precise outcomes within the initial hundred terms of the series.

The impacts of α_i on the EST and SPSC are demonstrated in Figs. 2 and 3 for Scenario-I.

It is observed that EST gradually increases with Ψ_Q. Similar observations are also seen in [58]. Again, as the non-linearity parameter increases, the communication link improves [5] (i.e. the link will undergo less amount of fading with higher α_i), hence the EST becomes better for lower α_p and α_e. On the other hand, as expected, the SPSC is enhanced as Φ_o and α_r increase from a lower to a higher value.

The SOP is plotted against Φ_p, Ψ_Q, and Φ_r considering Scenario-I in Figs. 4, 5, and 6, respectively, with a view to observing the impacts of the number of multipath clusters.

It can clearly be noted that the SOP performance is improved by Ψ_Q and Φ_r, and diminished by Φ_p as reported in [4]. This is as

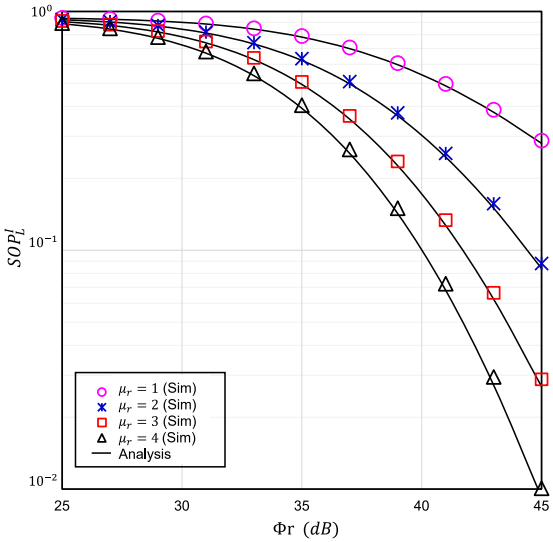

Fig. 6. The SOP versus Φ_r for selected values of μ_r with $\alpha_o = 2.296$, $\beta_o = 2$, $\Omega_o = 1$, $g = 2$, $\epsilon_o = 1$, $s = 1$, $\alpha_r = \alpha_p = \alpha_e = 2$, $\mu_p = \mu_e = 2$, $P_o = 0.1$, $\Phi_p = 15\,dB$, $\Phi_o = 10\,dB$, $\Phi_e = 15\,dB$, $\Psi_Q = -5\,dB$, and $\Upsilon_e = 0.05$ bits/sec/Hz.

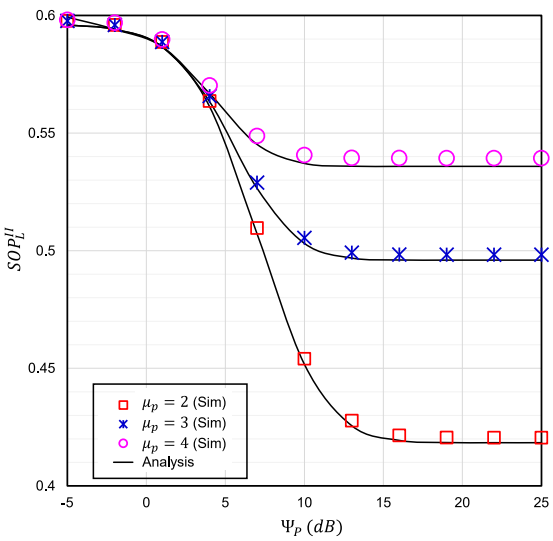

Fig. 7. The SOP versus Ψ_T for selected values of μ_p with $\alpha_o = 2.296$, $\beta_o = 2$, $\Omega_o = 1$, $g = 2$, $\epsilon = 6.7$, $P_o = 0.2$, $s = 1$, $\alpha_r = \alpha_p = \alpha_e = 2$, $\mu_r = \mu_e = 2$, $\Phi_p = -5\,dB$, $\mu_s = 10\,dB$, $\Phi_r = -5\,dB$, $\Psi_Q = 5\,dB$, $\Phi_e = 5\,dB$, and $\Upsilon_e = 0.05$ bits/sec/Hz.

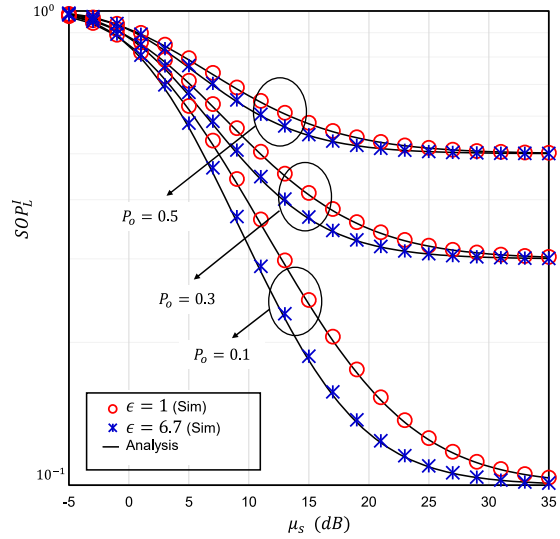

Fig. 8. The SOP versus μ_s for selected values of P_o and ϵ with $\alpha_o = 2.296$, $\beta_o = 2$, $\Omega_o = 1$, $g = 2$, $s = 1$, $\alpha_r = \alpha_p = \alpha_e = 2$, $\mu_r = \mu_p = \mu_e = 6$, $\Phi_r = \Phi_p = 15\,dB$, $\Phi_e = -5\,dB$, $\Psi_Q = -10\,dB$, and $\Upsilon_e = 0.05$ bits/sec/Hz.

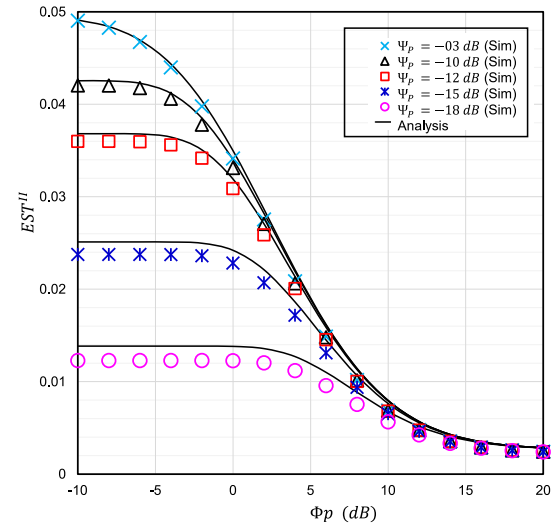

Fig. 9. The EST versus Φ_p for selected values of Ψ_T with $\alpha_o = 2.296$, $\beta_o = 2$, $\Omega_o = 1$, $g = 2$, $s = 2$, $\epsilon = 6.7$, $P_o = 0.1$, $\alpha_r = \alpha_p = \alpha_e = 2$, $\mu_r = \mu_p = \mu_e = 2$, $\Phi_o = -5\,dB$, $\Phi_r = 10\,dB$, $\Psi_Q = -10\,dB$, $\Phi_e = -5\,dB$, and $\Upsilon_e = 0.05$ bits/sec/Hz.

expected because the larger Ψ_Q indicates the higher transmitting power at S. On the other hand, Φ_r improves the $S - R$ RF sub-link while Φ_p strengthens the $S - P$ link. It is obvious that an increase in μ_i will increase the channel diversity thereby mitigating the channel fading. Therefore, the SOP decreases with μ_r and increases with μ_p and μ_e. Similar results were also demonstrated in [5] that corroborate the outcomes in this work. In Fig. 7, the impact of μ_p is demonstrated on SOP considering Scenario-II. Similar to Scenario-I, in this particular case, it is also observed that the SOP drastically degrades with μ_p.

In Fig. 8, the probability of link blockage is observed via plotting SOP against the average SNR of FSO link under various levels of pointing error. It is observed that the probability of link blockage imposes a significant impact on the SOP performance, that is, the SOP degrades with the increase in P_o (increased P_o signifies a stronger link blockage). It is obvious because similar to the observations in [6], the atmospheric turbulence degrades with the increase in link blockage, which yields to a degraded secrecy performance.

Fig. 9 depicts the impact of Ψ_T on the EST performance for Scenario-II. It can be noted that an increased Ψ_T is beneficial for EST performance since in that case the increased transmit power yields a better received SNR at the destination. After 15 dB, an error floor is observed, as expected. This occurs as the transmit power at S is limited by a threshold value.

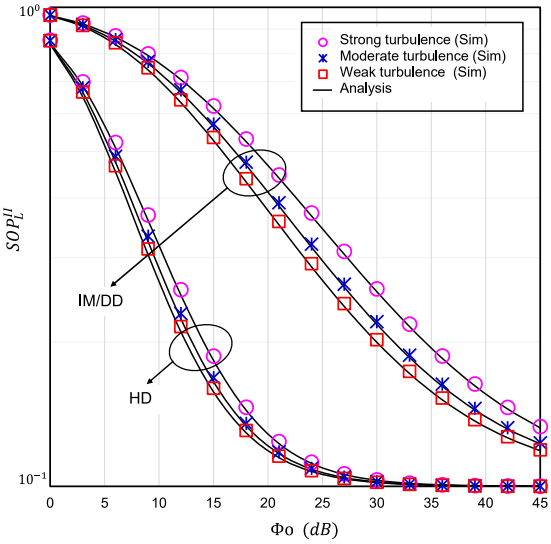

Fig. 10. The SOP versus Φ_o for selected values of α_o, β_o, and s with $\Omega_o = 1, g = 2, \epsilon = 6.7, P_o = 0.1, \alpha_r = \alpha_p = \alpha_e = 2, \mu_r = \mu_p = \mu_e = 6, \Phi_r = \Phi_p = 15\,dB$, $\Phi_e = -5\,dB$, $\Psi_T = \Psi_Q = -10\,dB$, and $\Upsilon_e = 0.05$ bits/sec/Hz.

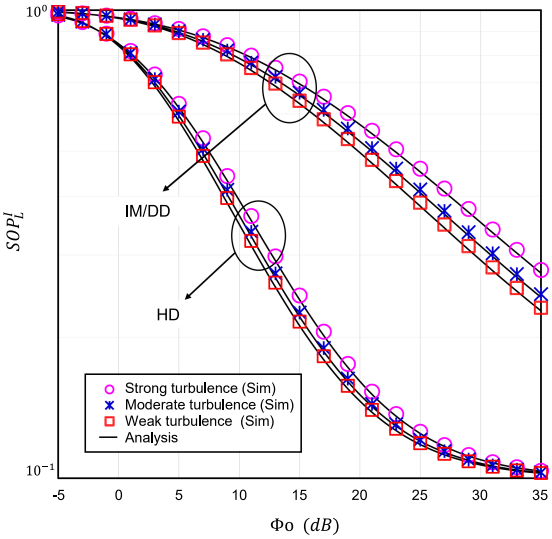

Fig. 11. The SOP versus Φ_o for selected values of α_o, β_o and s with $\Omega_o = 1$, $g = 2$, $\epsilon = 1$, $P_o = 0.1$, $\alpha_r = \alpha_p = \alpha_e = 2$, $\mu_r = \mu_p = \mu_e = 6, \Phi_r = \Phi_p = 15\,dB$, $\Phi_e = -5\,dB$, $\Psi_Q = -10\,dB$, and $\Upsilon_e = 0.05$ bits/sec/Hz.

The FSO link performance is significantly affected by atmospheric turbulence. Based on the values of α_o and β_o, three turbulence conditions (e.g. strong, moderate, and weak) are considered in this work. Figs. 10 and 11 demonstrate how the secrecy performance is affected by various turbulence conditions under Scenarios- I & II.

As stronger turbulence results in lower SNR at the destination, weaker turbulence leads to improved secrecy performance, as demonstrated in [32]. Moreover, a comparison between the two detection techniques is also presented that clearly reveals that the HD technique overcomes atmospheric turbulence more appropriately than the IM/DD technique. The results in [57] also completely match with this outcome.

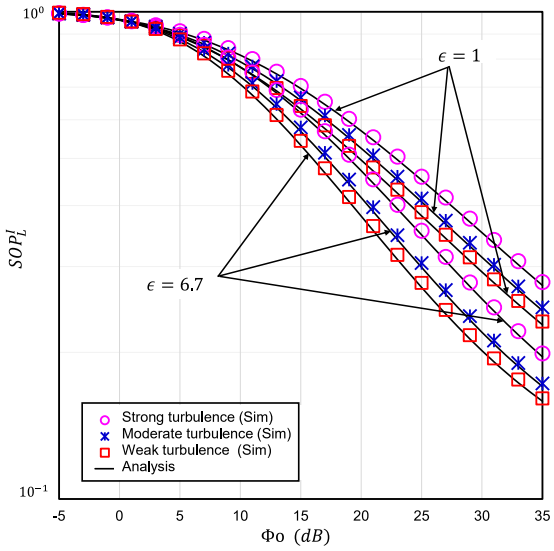

Fig. 12. The SOP versus Φ_o for selected values of α_o, β_o and ϵ with $\Omega_o = 1$, $g = 2$, $s = 2$, $P_o = 0.1$, $\alpha_r = \alpha_p = \alpha_e = 2$, $\mu_r = \mu_p = \mu_e = 6, \Phi_r = \Phi_p = 15\,dB$, $\Phi_e = -5\,dB$, $\Psi_Q = -10\,dB$, and $\Upsilon_e = 0.05$ bits/sec/Hz.

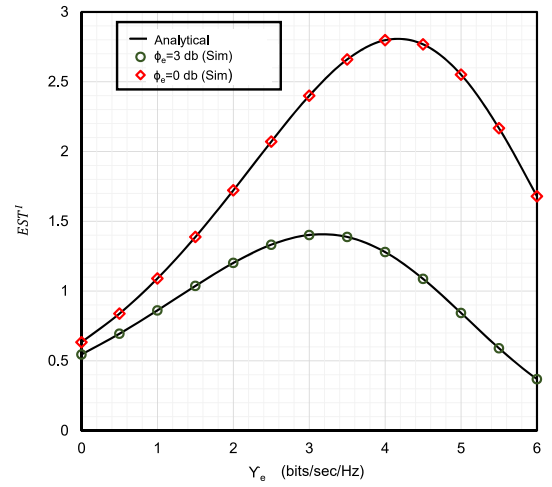

Fig. 13. The EST versus Υ_e for selected values of Φ_e with $\alpha_o = 2.296, \beta_o = 2, \Omega_o = 1, g = 2, \epsilon = 1, s = 2, P_o = 0.2, \alpha_r = \alpha_p = \alpha_e = 2$, $\mu_r = \mu_p = \mu_e = 6, \Phi_r = \Phi_p = 15\,dB, \Phi_e = -5\,dB$, and $\Psi_Q = -10\,dB$.

Besides the atmospheric turbulence, pointing error also plays a vital role in the FSO link performance that is illustrated in Fig. 12 by depicting SOP as a function of the average SNR of the FSO channel experiencing Scenario-I. The result exhibits that a higher pointing error (lower value of ϵ) is more detrimental for better SOP than a lower pointing error (higher value of ϵ). This happens since a lower pointing error designates a better-pointing accuracy that yields a better detection of the received signal. This statement can be easily justified with similar results presented in [57].

The purpose of plotting the EST against Υ_e in Fig. 13 is to examine the influence of changes in Υ_e on the system's secrecy performance. This graph also showcases the balance between the resources needed to keep the information secure and the rate at which confidential information can be transmitted. It

is noticed that a lower Υ_e exhibits in lower resources being required to maintain the desired secrecy level, resulting in larger EST performance. As Υ_e increases, the desired level of security will need more resources for the increased secrecy threats, hence the EST decreases.

VII. Conclusion

In this work, the secrecy performance of a CUN-based hybrid RF/FSO network has been investigated wherein both maximum transmit power and interference power constraints within the CR spectrum are taken into consideration. Assuming all the RF and FSO links are subjected to $\alpha-\mu$ fading and Málaga ($\mathcal{M}$) turbulence, respectively, the expressions of SOP, probability of SPSC, and EST are derived in closed-form. The tightness of the simulation and analytical results are also demonstrated via MC simulations. Furthermore, the impacts of the system parameters on the security performance are analyzed by capitalizing on the derived expressions. The results found from our analysis are as follows.

1) A slight increase in fading parameter of the main link can increase the system security significantly.
2) The variation in EST with the fading parameter (α) is almost linear until it reaches the maximum value.
3) For a similar amount of fading or atmospheric turbulence, IM/DD performs worse than the HD technique.
4) With the increase of the distance between the transmitter and receiver, the average SNR decreases, thereby diminishing the secrecy of the system under consideration.
5) The high chance of link obstruction and severe pointing error also remarkably deteriorate the secrecy of the system.

The validity of our result is further demonstrated by the Monte-Carlo simulation.

Appendix

A. Proof of Λ_2

Λ_2 is given as

$$\Lambda_2 = \underbrace{\int_{\frac{\Psi_Q}{\Psi_T}}^{\infty} \frac{\alpha_p \delta_p^{\mu_p}}{2\Gamma(\mu_p)} y^{\Theta_p} e^{-\delta_p y^{\tilde{\alpha_r}}} dy}_{\mathcal{P}_1} - \underbrace{\int_{\frac{\Psi_Q}{\Psi_T}}^{\infty} \sum_{m_r=0}^{\mu_r-1} \frac{\alpha_p \delta_p^{\mu_p}}{2\Gamma(\mu_p)} \frac{\delta_r^{m_r}}{m_r!} \frac{\Psi_Q^{-\tilde{\alpha_r} m_r} \gamma_r^{\tilde{\alpha_r} m_r} y^{\Theta_p + \tilde{\alpha_r} m_r}}{e^{(\delta_p y^{\tilde{\alpha_r}} + \delta_r \Psi_Q^{-\tilde{\alpha_r}} \gamma_r^{\tilde{\alpha_r}} y^{\tilde{\alpha_r}})}} dy}_{\mathcal{P}_2}.$$

By using [42, Eq. (3.381.9)], $\mathcal{P}_1$ is expressed as

$$\mathcal{P}_1 = \frac{\alpha_p \delta_p^{\mu_p}}{2\Gamma(\mu_p)} \int_{\frac{\Psi_Q}{\Psi_T}}^{\infty} y^{\Theta_p} e^{-\delta_p y^{\tilde{\alpha_r}}} dy = \Xi_5^{II}.$$

$\mathcal{P}_2$ is written as

$$\mathcal{P}_2 = \sum_{m_r=0}^{\mu_r-1} \frac{\alpha_p \delta_p^{\mu_p} \delta_r^{m_r}}{2\Gamma(\mu_p) m_r!} \Psi_Q^{-\tilde{\alpha_r} m_r} \gamma_r^{\tilde{\alpha_r} m_r} \int_{\frac{\Psi_Q}{\Psi_T}}^{\infty} y^{\Theta_p + \tilde{\alpha_r} m_r} \times e^{-\delta_p y^{\tilde{\alpha_r}}} e^{-\delta_r \Psi_Q^{-\tilde{\alpha_r}} \gamma_r^{\tilde{\alpha_r}} y^{\tilde{\alpha_r}}} dy. \quad (52)$$

Due to tractable analysis, assuming $\tilde{\alpha_p} = \tilde{\alpha_r}$ and using similar formula as for $\mathcal{P}_1$, $\mathcal{P}_2$ is expressed as

$$\mathcal{P}_2 = \sum_{m_r=0}^{\mu_r-1} \frac{\alpha_p \delta_p^{\mu_p} \delta_r^{m_r}}{2\Gamma(\mu_p) m_r!} \Psi_Q^{-\tilde{\alpha_r} m_r} \gamma_r^{\tilde{\alpha_r} m_r} \int_{\frac{\Psi_Q}{\Psi_T}}^{\infty} y^{\Theta_p + \tilde{\alpha_r} m_r} \times e^{-y^{\tilde{\alpha_r}} (\delta_p + \delta_r \Psi_Q^{-\tilde{\alpha_r}} \gamma_r^{\tilde{\alpha_r}})} dy = \sum_{m_r=0}^{\mu_r-1} \frac{\alpha_p \delta_p^{\mu_p} \delta_r^{m_r}}{2\Gamma(\mu_p) m_r!} \times \Psi_Q^{-\tilde{\alpha_r} m_r} \gamma_r^{\tilde{\alpha_r} m_r} \frac{\Gamma\left[\Omega, \left(\delta_p + \delta_r \Psi_T^{-\tilde{\alpha_r}} \gamma_r^{\tilde{\alpha_r}}\right) \left(\frac{\Psi_Q}{\Psi_T}\right)^{\tilde{\alpha_r}}\right]}{\tilde{\alpha_r} (\delta_p + \delta_r \Psi_Q^{-\tilde{\alpha_r}} \gamma_r^{\tilde{\alpha_r}})^{\Omega}}.$$

Utilizing the integral formula of [42, Eq. (8.352.7)] and performing some mathematical manipulations, $\mathcal{P}_2$ is demonstrated in an alternative form as

$$\mathcal{P}_2 = \sum_{m_r=0}^{\mu_r-1} \sum_{m_3=0}^{\Omega-1} \sum_{m_4=0}^{m_3} \sum_{m_5=0}^{\infty} \binom{m_3}{m_4} \binom{\Omega + m_5 - 1}{m_5} \times \Xi_6^{II} \gamma_r^{\tilde{\alpha_r}(m_r + m_4 + m_5)} e^{-(\delta_p \Psi_Q^{\tilde{\alpha_r}} \Psi_T^{-\tilde{\alpha_r}} + \delta_r \Psi_T^{-2\tilde{\alpha_r}} \Psi_Q^{\tilde{\alpha_r}} \gamma_r^{\tilde{\alpha_r}})}. \quad (53)$$

References

[1] S. Haykin, "Cognitive radio: Brain-empowered wireless communications," *IEEE J. Sel. Areas Commun.*, vol. 23, no. 2, pp. 201–220, Feb. 2005.

[2] I. S. Ansari, L. Jan, Y. Tang, L. Yang, and M. H. Zafar, "Outage and error analysis of dual-hop TAS/MRC MIMO RF-UOWC systems," *IEEE Trans. Veh. Technol.*, vol. 70, no. 10, pp. 10093–10104, Oct. 2021.

[3] I. S. Ansari, M. M. Abdallah, M.-S. Alouini, and K. A. Qaraqe, "A performance study of two hop transmission in mixed underlay RF and FSO fading channels," in *Proc. IEEE Wireless Commun. Netw. Conf.*, 2014, pp. 388–393.

[4] E. Erdogan, N. Kabaoglu, I. Altunbas, and H. Yanikomeroglu, "On the error probability of cognitive RF-FSO relay networks over Rayleigh/EW fading channels with primary-secondary interference," *IEEE Photon. J.*, vol. 12, no. 1, pp. 1–13, Feb. 2020.

[5] N. H. Juel et al., "Secrecy performance analysis of mixed α-μ and exponentiated weibull RF-FSO cooperative relaying system," *IEEE Access*, vol. 9, pp. 72342–72356, 2021.

[6] G. T. Djordjevic, M. I. Petkovic, M. Spasic, and D. S. Antic, "Outage capacity of FSO link with pointing errors and link blockage," *Opt. Exp.*, vol. 24, no. 1, pp. 219–230, 2016.

[7] I. S. Ansari, F. Yilmaz, and M.-S. Alouini, "On the performance of hybrid RF and RF/FSO dual-hop transmission systems," in *Proc. IEEE 2nd Int. Workshop Opt. Wireless Commun.*, 2013, pp. 45–49.

[8] B. Makki, T. Svensson, T. Eriksson, and M.-S. Alouini, "On the performance of RF-FSO links with and without hybrid ARQ," *IEEE Trans. Wireless Commun.*, vol. 15, no. 7, pp. 4928–4943, Jul. 2016.

[9] M. N. Khan and M Jamil, "Adaptive hybrid free space optical/radio frequency communication system," *Telecommun. Syst.*, vol. 65, no. 1, pp. 117–126, 2017.

[10] M. Usman, H.-C. Yang, and M.-S. Alouini, "Practical switching-based hybrid FSO/RF transmission and its performance analysis," *IEEE Photon. J.*, vol. 6, no. 5, pp. 1–13, Oct. 2014.

[11] H. Kaushal and G. Kaddoum, "Optical communication in space: Challenges and mitigation techniques," *IEEE Commun. Surv. Tut.*, vol. 19, no. 1, pp. 57–96, Firstquarter 2017.

[12] B. Bag, A. Das, I. S. Ansari, A. Prokeš, C. Bose, and A. Chandra, "Performance analysis of hybrid FSO systems using FSO/RF-FSO link adaptation," *IEEE Photon. J.*, vol. 10, no. 3, pp. 1–17, Jun. 2018.

[13] L. Yang, M. O. Hasna, and I. S. Ansari, "Unified performance analysis for multiuser mixed η-μ and $\mathcal{M}$-distribution dual-hop RF/FSO systems," *IEEE Trans. Commun.*, vol. 65, no. 8, pp. 3601–3613, Aug. 2017.

[14] P. K. Singya, N. Kumar, V. Bhatia, and M.-S. Alouini, "On the performance analysis of higher order QAM schemes over mixed RF/FSO systems," *IEEE Trans. Veh. Technol.*, vol. 69, no. 7, pp. 7366–7378, Jul. 2020.

[15] I. S. Ansari, M. M. Abdallah, M.-S. Alouini, and K. A. Qaraqe, "Outage analysis of asymmetric RF-FSO systems," in *Proc. IEEE 84th Veh. Technol. Conf.*, 2016, pp. 1–6.

[16] K. O. Odeyemi and P. A. Owolawi, "Selection combining hybrid FSO/RF systems over generalized induced-fading channels," *Opt. Commun.*, vol. 433, pp. 159–167, 2019.

[17] W. M. R. Shakir, "On performance analysis of hybrid FSO/RF systems," *IET Commun.*, vol. 13, no. 11, pp. 1677–1684, 2019.

[18] N. Varshney and A. K. Jagannatham, "Cognitive decode-and-forward MIMO-RF/FSO cooperative relay networks," *IEEE Commun. Lett.*, vol. 21, no. 4, pp. 893–896, Apr. 2017.

[19] A. M. Cvetković, V. M. Blagojević, and P. N. Ivaniš, "Outage performance of cognitive RF/FSO system with MRC scheme at the receiver," *Facta Universitatis, Series: Autom. Control Robot.*, vol. 14, no. 3, pp. 205–217, 2015.

[20] H. Arezumand, H. Zamiri-Jafarian, and E. Soleimani-Nasab, "Outage and diversity analysis of underlay cognitive mixed RF-FSO cooperative systems," *J. Opt. Commun. Netw.*, vol. 9, no. 10, pp. 909–920, 2017.

[21] N. Varshney, A. K. Jagannatham, and P. K. Varshney, "Cognitive MIMO-RF/FSO cooperative relay communication with mobile nodes and imperfect channel state information," *IEEE Trans. Cogn. Commun. Netw.*, vol. 4, no. 3, pp. 544–555, Sep. 2018.

[22] F. S. Al-Qahtani, A. H. A. El-Malek, I. S. Ansari, R. M. Radaydeh, and S. A. Zummo, "Outage analysis of mixed underlay cognitive RF MIMO and FSO relaying with interference reduction," *IEEE Photon. J.*, vol. 9, no. 2, pp. 1–22, Apr. 2017.

[23] M. Ibrahim, A. Badrudduza, M. Hossen, M. K. Kundu, and I. S. Ansari, "Enhancing security of TAS/MRC based mixed RF-UOWC system with induced underwater turbulence effect," *IEEE Syst. J.*, vol. 16, no. 4, pp. 5584–5595, Dec. 2022.

[24] L. Yang, M. O. Hasna, and I. S. Ansari, "Physical layer security for TAS/MRC systems with and without co-channel interference over η-μ fading channels," *IEEE Trans. Veh. Technol.*, vol. 67, no. 12, pp. 12421–12426, Dec. 2018.

[25] M. T. Tania, M. Ibrahim, M. S. Hossen, A. S. M. Badrudduza, and M. K. Kundu, "Combined impacts of co-channel interference and correlation on secrecy performance over $\kappa - \mu$ shadowed fading channel," in *Proc. IEEE Int. Conf. Advance. Elect. Electron. Eng.*, 2022, pp. 1–6.

[26] W. M. R. Shakir, "Physical layer security performance analysis of hybrid FSO/RF communication system," *IEEE Access*, vol. 9, pp. 18948–18961, 2021.

[27] A. S. M. Badrudduza et al., "Security at the physical layer over GG fading and mEGG turbulence induced RF-UOWC mixed system," *IEEE Access*, vol. 9, pp. 18123–18136, 2021.

[28] Y. Ai, A. Mathur, H. Lei, M. Cheffena, and I. S. Ansari, "Secrecy enhancement of RF backhaul system with parallel FSO communication link," *Opt. Commun.*, vol. 475, 2020, Art. no. 126193.

[29] M. Kafafy, Y. Fahmy, M. Khairy, and M. Abdallah, "Secure backhauling over adaptive parallel mmWave/FSO link," in *Proc. IEEE Int. Conf. Commun. Workshops*, 2020, pp. 1–6.

[30] N. A. Sarker et al., "Secrecy performance analysis of mixed hyper-gamma and gamma-gamma cooperative relaying system," *IEEE Access*, vol. 8, pp. 131273–131285, 2020.

[31] H. Lei, H. Luo, K. Park, Z. Ren, G. Pan, and M. Alouini, "Secrecy outage analysis of mixed RF-FSO systems with channel imperfection," *IEEE Photon. J.*, vol. 10, no. 3, pp. 1–13, Jun. 2018.

[32] S. H. Islam et al., "On secrecy performance of mixed generalized Gamma and Málaga RF-FSO variable gain relaying channel," *IEEE Access*, vol. 8, pp. 104127–104138, 2020.

[33] K. O. Odeyemi, P. A. Owolawi, and O. O. Olakanmi, "Secrecy performance of cognitive underlay hybrid RF/FSO system under pointing errors and link blockage impairments," *Opt. Quantum Electron.*, vol. 52, no. 3, pp. 1–16, 2020.

[34] D. R. Pattanayak, V. K. Dwivedi, and V. Karwal, "On the physical layer security of hybrid RF-FSO system in presence of multiple eavesdroppers and receiver diversity," *Opt. Commun.*, vol. 477, 2020, Art. no. 126334.

[35] S. C. Tokgoz, S. Althunibat, S. L. Miller, and K. A. Qaraqe, "On the secrecy capacity of hybrid FSO-mmWave wiretap channels," *IEEE Trans. Veh. Technol.*, vol. 71, no. 4, pp. 4073–4086, Apr. 2022.

[36] M. D. Yacoub, "The α-μ distribution: A physical fading model for the Stacy distribution," *IEEE Trans. Veh. Technol.*, vol. 56, no. 1, pp. 27–34, Jan. 2007.

[37] S. H. Islam et al., "Impact of correlation and pointing error on secure outage performance over arbitrary correlated Nakagami-m and $\mathcal{M}$-turbulent fading mixed RF-FSO channel," *IEEE Photon. J.*, vol. 13, no. 2, pp. 1–17, Apr. 2021.

[38] A. Afana, I. A. Mahady, and S. Ikki, "Quadrature spatial modulation in MIMO cognitive radio systems with imperfect channel estimation and limited feedback," *IEEE Trans. Commun.*, vol. 65, no. 3, pp. 981–991, Mar. 2017.

[39] H. Lei, I. S. Ansari, G. Pan, B. Alomair, and M.-S. Alouini, "Secrecy capacity analysis over $\alpha - \mu$ fading channels," *IEEE Commun. Lett.*, vol. 21, no. 6, pp. 1445–1448, Jun. 2017.

[40] M. D. Yacoub, "The α-μ distribution: A physical fading model for the Stacy distribution," *IEEE Trans. Veh. Technol.*, vol. 56, no. 1, pp. 27–34, Jan. 2007.

[41] L. Kong, S. Vuppala, and G. Kaddoum, "Secrecy analysis of random MIMO wireless networks over α-μ fading channels," *IEEE Trans. Veh. Technol.*, vol. 67, no. 12, pp. 11654–11666, Dec. 2018.

[42] I. S. Gradshteyn and I. M. Ryzhik, *Table of Integrals, Series, and Products*. 7th ed. San Diego, CA, USA: Academic, 2007.

[43] G. Xu and Z. Song, "Performance analysis for mixed $\kappa - \mu$ fading and m-distribution dual-hop radio frequency/free space optical communication systems," *IEEE Trans. Wireless Commun.*, vol. 20, no. 3, pp. 1517–1528, Mar. 2021.

[44] A. A. Ibrahim et al., "Performance analysis of free space optical communication systems over imprecise Málaga fading channels," *Opt. Commun.*, vol. 457, 2020, Art. no. 124694.

[45] I. S. Ansari, F. Yilmaz, and M.-S. Alouini, "Performance analysis of free-space optical links over Málaga ($\mathcal{M}$) turbulence channels with pointing errors," *IEEE Trans. Wireless Commun.*, vol. 15, no. 1, pp. 91–102, Jan. 2016.

[46] A. Prudnikov, Y. Brychkov, and O. Marichev, *Integrals and Series: More Special Functions*, vol. 3. Philadelphia, PA, USA: Gordon And Breach Science Publishers, 1992.

[47] "The mathematical functions site." Accessed: Jul. 23, 2021. [Online]. Available: https://functions.wolfram.com/

[48] A. Papoulis and H. Saunders, *Probability, Random Variables and Stochastic Processes*. New York, NY, USA: Tata McGraw-Hill 1989.

[49] H. Lei et al., "Performance analysis of physical layer security over generalized-K fading channels using a mixture gamma distribution," *IEEE Commun. Lett.*, vol. 20, no. 2, pp. 408–411, Feb. 2016.

[50] T. Hossain, S. Shabab, A. S. M. Badrudduza, M. K. Kundu, and I. S. Ansari, "On the physical layer security performance over RIS-aided dual-hop RF-UOWC mixed network," *IEEE Trans. Veh. Technol.*, vol. 72, no. 2, pp. 2246–2257, Feb. 2023.

[51] M. Ibrahim, M. Z. I. Sarkar, A. S. M. Badrudduza, M. K. Kundu, and S. Dev, "Impact of correlation on the security in multicasting through κ - μ shadowed fading channels," in *Proc. IEEE Region 10 Symp.*, 2020, pp. 1396–1399.

[52] V. Adamchik and O. Marichev, "The algorithm for calculating integrals of hypergeometric type functions and its realization in reduce system," in *Proc. Int. Symp. Symbolic Algebr. Computation*, 1990, pp. 212–224.

[53] J. M. Moualeu, D. B. da Costa, W. Hamouda, U. S. Dias, and R. A. de Souza, "Physical layer security over $\alpha - \kappa - \mu$ and $\alpha - \eta - \mu$ fading channels," *IEEE Trans. Veh. Technol.*, vol. 68, no. 1, pp. 1025–1029, Jan. 2019.

[54] M. D. Springer, *The Algebra of Random Variables*. New York, NY, USA: Wiley, 1979.

[55] P. Mittal and K. Gupta, "An Integral Involving Generalized Function of Two Variables," in *Proc. Indian Acad. Sci.-Sect. A*, 1972, pp. 117–123.

[56] A. M. Mathai, R. K. Saxena, and H. J. Haubold, *The H-Function: Theory and Applications*. Berlin, Germany: Springer, 2009.

[57] H. Lei et al., "On secure mixed RF-FSO systems with TAS and imperfect CSI," *IEEE Trans. Commun.*, vol. 68, no. 7, pp. 4461–4475, Jul. 2020.

[58] H. Lei et al., "Secrecy outage performance for SIMO underlay cognitive radio systems with generalized selection combining over Nakagami-m channels," *IEEE Trans. Veh. Technol.*, vol. 65, no. 12, pp. 10126–10132, Dec. 2016.